Pacific Gas and Electric Company™

Gregory M. Rueger
Senior Vice President–
Generation and
Chief Nuclear Officer

US Mail:
Mail Code B32
Pacific Gas and Electric Company
PO Box 770000
San Francisco, CA 94177-0001

Overnight Mail:
Mail Code B32
Pacific Gas and Electric Company
77 Beale Street, 32nd Floor
San Francisco, CA 94105-1814

415.973.4684
Fax: 415.973.2313

March 11, 2002

PG&E Letter DCL-02-023

U.S. Nuclear Regulatory Commission
ATTN: Document Control Desk
Washington, DC 20555-0001

Docket No. 50-275, OL-DPR-80
Docket No. 50-323, OL-DPR-82
Diablo Canyon Units 1 and 2
Response to NRC Request for Additional Information Regarding Supplement 3 to License Amendment Request 00-06, "Alternate Repair Criteria for Axial PWSCC at Dented Intersections in Steam Generator Tubing"

Dear Commissioners and Staff:

On February 6 and February 19, 2002, the NRC staff identified additional information required in order to complete its evaluation associated with Supplement 3 to License Amendment Request (LAR) 00-06. LAR 00-06 proposes Technical Specification changes to incorporate alternate repair criteria for axial primary water stress corrosion cracking (PWSCC) at dented steam generator tube support plate locations. LAR 00-06 was submitted to the NRC in PG&E Letter DCL-01-110, "Supplement 3 to License Amendment Request 00-06, 'Alternate Repair Criteria for Axial PWSCC at Dented Intersections in Steam Generator Tubing,'" dated November 13, 2001. A response to a prior NRC request for additional information on LAR 00-06 was submitted in PG&E Letter DCL-02-019, "Response to NRC Request for Additional Information Regarding Supplement 3 to License Amendment Request 00-06, "Alternate Repair Criteria for Axial PWSCC at Dented Intersections in Steam Generator Tubing,'" dated February 26, 2002. PG&E's response to the request for additional information received on February 6 and February 19, 2002, is included in Enclosures 1 and 2.

This additional information does not affect the results of the safety evaluation and no significant hazards determination previously transmitted in PG&E Letter DCL-01-110.

A001

Figures 18a, 18b, 19a, and 19b contained in Enclosure 2 have been reproduced from Figures G-14 and G-15 contained in Appendix G of Electric Power Research Institute (EPRI) Report TR-107197-P2, "Depth Based Structural Analysis Methods for SG Circumferential Indications," dated December 1997. EPRI Report TR-107197-P2 is a licensed product.

If you have any questions regarding this response, please contact Patrick Nugent at (805) 545-4720.

Sincerely,

Gregory M. Rueger
Senior Vice President – Generation and Chief Nuclear Officer

kjs/4328
Enclosure
cc/enc: Edgar Bailey, DHS
Girija S. Shukla
Ellis W. Merschoff
David L. Proulx

UNITED STATES OF AMERICA
NUCLEAR REGULATORY COMMISSION

In the Matter of PACIFIC GAS AND ELECTRIC COMPANY	)	Docket No. 50-275 Facility Operating License No. DPR-80
Diablo Canyon Power Plant Units 1 and 2	)	Docket No. 50-323 Facility Operating License No. DPR-82

AFFIDAVIT

Gregory M. Rueger, of lawful age, first being duly sworn upon oath says that he is Senior Vice President - Generation and Chief Nuclear Officer of Pacific Gas and Electric Company; that he has executed this response to the request for additional information on Supplement 3 to License Amendment Request 00-06 on behalf of said company with full power and authority to do so; that he is familiar with the content thereof; and that the facts stated therein are true and correct to the best of his knowledge, information, and belief.

Gregory M. Rueger
Senior Vice President – Generation
and Chief Nuclear Officer

Subscribed and sworn to before me this 11th day of March 2002.
County of San Francisco
State of California

Notary Public

AMY EMIKO DONG
Commission # 1206749
Notary Public - California
San Francisco County
My Comm. Expires Jan 2, 2003

PG&E Response to NRC Request for Additional Information Regarding Supplement 3 to License Amendment Request 00-06, "Alternate Repair Criteria for Axial PWSCC at Dented Intersections in Steam Generator Tubing"

Questions on Utilization of New Growth Data Based Entirely On Diablo Canyon Data

Question A.1

On page 4-19 (Section 4.7.1) of WCAP-15573, Revision 1, it was indicated that growth data are obtained from Cycles 8 to 10 for Diablo Canyon Units 1 and 2. Does this mean that 3 successive cycles of data are available and used to obtain the growth rates or does this mean that there are 2 cycles of data from 3 outages? With respect to the data in Table 4-7, has the data from only one pair of successive outages (i.e., one cycle) been used to obtain the growth rates? If so, which pair/cycle (e.g., outages 8 and 9 or outages 9 and 10) is actually used in the analysis. If data from only one pair of consecutive outages (i.e., one cycle) is used, discuss how the data from the other pair of consecutive outages (i.e., cycle) compares. If data from both pairs of consecutive outages (outages 8 and 9 and outages 9 and 10) are used, discuss whether the growth rates from the two are comparable.

PG&E Response to Question A.1

Growth data have been obtained from three successive cycles in each unit for a total of six cycles of growth data (i.e. Unit 1 Cycle 8, Unit 1 Cycle 9, Unit 1 Cycle 10, Unit 2 Cycle 8, Unit 2 Cycle 9, and Unit 2 Cycle 10). Upon reviewing the growth data in WCAP-15573, Revision 1, some errors were found in the data of Table 4-7. The corrected table is enclosed in this letter as Table 4-7R1. A modified Table 4-8R1 and modified Figure 4-14R1, Figure 4-15R1, and Figure 4-16R1 are also included. The first column of Table 4-7R1 identifies the end of cycle (EOC) outage for each growth rate indication. For example, 1R8 identifies a growth rate obtained from Unit 1 Cycle 8 (Unit 1 Refueling Outage 8 and Unit 1 Refueling Outage 7 data). The cumulative growth distributions of Table 4-8R1 are developed from the six cycles of growth data given in Table 4-7R1. For the modified Table 4-8R1, growth data for cycles with growth rates toward the lower end of the combined data for all cycles were excluded from the distributions as described in Table 4-8R1 and the Titles to Figures 4-14R1 to 4-16R1. This increases the conservatism in the growth distributions compared to that obtained from the sum of all six cycles.

Although the individual cycle populations are small (ranging from 14 to 83 growth values), cumulative distributions for each of the six cycles can be compared as shown in Figure 1, enclosed in this letter, for growth in average depth and Figure 2 for growth in length. The figures also include the combined growth distributions of Table 4-8R1 as a lined curve. The combined growth distributions were developed from the cycles with larger growth rates. Variations between cycles are reasonable for the small populations of indications. The less conservative cycles of growth data have been excluded from

the growth distributions of Table 4-8R1 (as indicated in the column headings on Table 4-8R1) in order to eliminate the influence of a large number of negative and non-conservative values in the cumulative probabilities. In general, the growth distributions for the operational assessments will be based upon combining growth data for the three or four cycles with the largest growth rates. When 200 growth values are obtained for each unit, the growth distributions may be separately defined for each unit if any significant differences are found between the units.

The combined distributions of Table 4-8R1 are planned for application at the next Unit 1 inspection, Unit 1 Refueling Outage 11 (1R11). The 1R11 data will be used to update the overall growth database. This update includes deleting the oldest data such that the 1R8 and 2R8 data would be excluded from consideration in the next update. Following the 1R11 outage, the distribution for the Unit 2 Refueling Outage 11 (2R11) outage will be defined. Since the 2R10 growth data have the largest tails for the growth distributions, it is anticipated that the growth from this cycle may have to be used at 2R11 rather than the combined distribution.

Question A.2

Growth rates are derivative quantities because they are derived from two independent measurements. When derivative quantities are obtained, the uncertainty in the results is increased beyond that of the uncertainty in the original measurements. That uncertainty is reflected in the growth rates presented in Table 4-7. Therefore, the growth rate distribution is expected to be broad due to the increased uncertainty associated with the derivative quantity. This increased uncertainty may be partly responsible for the negative growth rates obtained. There is a significant fraction of the data that give rise to negative growth rates. It was indicated that in preparing the growth rate cumulative probability fraction (CPF), negative growth rates are set to zero. In calculating the average growth rate and other statistics in Table 4-7, are the negative growth rates set to zero before calculating the various quantities?

PG&E Response to Question A.2

The two inspection results contributing to a growth rate should not be considered as two independent measurements for uncertainty considerations. Since the two signals are frequently very similar for small growth rates, the technique error (depth from phase versus truth) is essentially the same for both measurements. Differences in analyst variability are also minimized due to the similarity of the signals. In some cases, the same analyst evaluates the data from both inspections, which tends to minimize the random errors. Monte Carlo simulations are frequently applied to estimate "true growth" based on adjustments for nondestructive examination (NDE) uncertainties from the growth data obtained from two EOC NDE analyses. Based upon observations from these Monte Carlo simulations, the mean NDE sizing error is essentially eliminated for the growth data and the resulting uncertainty on the growth data is typically near the standard error for one measurement. The "true growth" generally results in smaller growth rates than obtained from the two EOC NDE analyses.

The negative growth rates (not set to zero) are appropriately included in the average growth values given at the end of Table 4-7R1. The uncertainties on the growth rates are assumed to be represented by symmetrical distributions, and the best estimate for the average growth is obtained by including the negative growth values. The 95th percentile values represent the upper 95th percentile of all data including the negative values.

Question A.3

It was indicated that the plots in Figures 4-14, 4-15, and 4-16 of WCAP 15573, Revision 1, include the growth distribution data of Table 4-8 as well as the data points of Table 4-7. In what sense are the data points of Table 4-7 included in the plots of Figures 4-14, 4-15, and 4-16? From the Figures it appears that the data points in Table 4-7 are used to construct CPF without setting the negative growth rates to zero and the results are plotted in the appropriate figures. If this is the case, either the legends or the y-axes in all these figures appear misleading. Please clarify what is represented in Figures 4-14, 4-15, and 4-16 and what distributions will be used in the tube integrity analysis. Is there a reason for presenting the CPF with/without setting the negative growth rates to zero?

PG&E Response to A.3

The data points of Table 4-7 were ordered from lowest to highest and plotted as a CPF including the negative values in Figures 4-14 to 4-16. The CPF growth distributions of Table 4-8 represent a smoothed fit to the growth data in the figures with negative growth rates set to zero growth. With the exception of voltage, these CPF growth distributions are updated during and/or after each inspection for application in Monte Carlo assessments. The legends in Figures 4-14 to 4-16 define the symbols (i.e., average and maximum depth growth/EFPY) for the data points and the lines in the plots and represent the CPF growth distributions of Table 4-8. The legends and y-axis labels are correct, and no further clarification should be necessary. The CPF plots in Figures 4-14 to 4-16 were intended to show all growth data and thus include the negative growth values.

Questions Related to Burst Testing and Leak Rate Analysis
in WCAP-15573, Revision 1

Question B.1

In Section 4.7.1 of WCAP-15573, Revision 1, (page 4-18), it was indicated that in some cases calls from previous inspection data must be forced to identify flaws because of the low signal strength for the previous cycle data. These "forced" calls would be used in determining flaw growth rates. Please provide more details on the re-analysis of prior cycle inspection data. In particular, address whether bias is introduced when calls are forced. If bias is introduced, discuss why this is appropriate. In Section 4.7.1 of

WCAP-15573, Revision 1, (page 4-19), on indication growth rate analysis, it states that in some cases the prior cycle indication was too small to be detected or sized; however when the later cycle indication was large, the prior cycle data could be sized. Discuss how the prior cycle indication was sized? Discuss the possibility that cracks initiate in mid-cycle and for some reason grow in an accelerated fashion. Discuss the need for special procedures to address these types of indications.

Response to Question B.1

When an indication is found that was not reported in the prior inspection, the prior inspection data is reanalyzed as part of the growth evaluation using the same depth profiling techniques that are used in the current outage. The term "forced" is used to imply that a prior inspection call is made whenever feasible using hindsight based on knowledge of the flaw location found in the later inspection. There is no reason to believe that this process introduces any bias in the NDE calls. For some indications, the prior cycle reanalysis may indicate that the presence of a flaw is probable even though no sizing can be performed. For some other indications, no flaw may be detectable and the indication would be considered no detectable degradation (NDD) in the reanalysis. In this case, the indication at the prior cycle may be present below detectable levels or the indication could have initiated during the cycle. As noted in Section 4.7.1 of WCAP-15573, Revision 1, these indications did not contribute to the largest indications found at the EOC inspection. There is no data to suggest that these indications initiated in midcycle followed by an accelerated growth while still representing small indications when detected at the EOC inspection. While no absolute statement on initiation time and growth can be made, it is clear that indications of this type tracked over successive cycles have the growth rates included in the growth distribution, which shows no abnormally large growth rates. Given the long term history (6 cycles of indications) of axial primary water stress corrosion cracking (PWSCC) at Diablo Canyon with no indications found to grow from NDD by reanalysis to large EOC indications, there is no need to have special procedures to address this type of indication.

Question B.2

The PWSCC growth rate data for Diablo Canyon is listed in Table 4-7 of WCAP-15573, Revision 1, and is plotted without any reference to their depth. Do the growth rate data show any correlation with depth? For example, are the deeper cracks on the average growing faster than shallower ones? If there is a depth dependence on growth rate, discuss the need to modify the tube integrity analysis (i.e., Monte Carlo procedures) for accounting for such depth dependence. If crack growth rates are dependent on depth, then only cracks of the same or similar depths should be used in the data set to construct the CPF. Is this taken into account in Section 4.7.1 and the subsequent Monte Carlo analysis in WCAP-15573, Revision 1? If not, has it been determined that the growth rate CPF being used is insensitive to depth or that it is conservative?

Response to Question B.2

Figures 3 to 5 enclosed in this letter show growth in average depth, length, and voltage as a function of the BOC values for each growth value excluding Unit 1 Refueling Outage 8 (1R8) results. 1R8 values were not included as the large number of negative growth values would tend to distort interpretation of the data for the later cycles of data. In all cases, there are no trends that show larger indications grow faster than smaller indications. In fact, the overall trend is toward decreasing growth with increasing BOC indications. The growth tends toward negative values for the larger BOC values such as average depth in Figure 3. This may reflect the small indications that are over-sized from the prior inspection data. The prior inspection population that may have been sized more accurately or undersized would have the smaller BOC values and the larger positive growth values. Since the growth distributions can be adequately applied as independent of BOC depth, they can be used in the Monte Carlo analyses with no need for modifications to the analysis process for dependence of growth in depth on the BOC depth.

Question B.3

In paragraph 5.5.3 on page 5-20 of WCAP-15573, Revision 1, it is stated that axial through-wall cracks ≤0.53-inch in length have burst pressures which exceed $1.4\Delta P_{SLB}$ by 15 percent, and all mixed mode indications with circumferential cracks with average depths ≤ 80 percent through-wall and axial through-wall lengths less than 0.53-inch would satisfy the burst margin. In Figure 5-10 (L shape, filled square symbols), the data for 0.48-inch long through-wall axial cracks in combination with a circumferential crack with an 80 percent through-wall depth shows that the reduction in burst pressure is 35 percent (i.e., the burst pressure for this mixed mode indication is 0.65 times the burst pressure of a 0.48-inch long single axial through-wall crack).

If this latter data were used to re-construct Figure 5-11, it appears the critical axial flaw sizes where the burst pressure may be reduced as a result of a circumferential flaw with average depths ≤80 percent would be different. For example, the burst pressure of a single 0.48-inch long though-wall crack is 4.5 ksi, implying that the mixed mode burst pressure would be 2.9 ksi (i.e., 0.65 x 4.5), which is significantly below $1.4\Delta P_{SLB}$. For an axial crack length of 0.48-inch, the axial crack depth where the ligament rupture pressure equals $1.4\Delta P_{SLB}$ would be approximately 82 percent. Thus any 0.48-inch long part-through-wall crack with a depth greater than 82 percent through-wall will have a burst pressure less than $1.4\Delta_{PSLB}$ if it is interacting with an 80 percent through-wall circumferential crack. If the triangular white area in Figure 5-11 were re-plotted based on this analysis, it would extend from 0.64-inch to at least 0.48-inch and 76 percent to some depth greater than 80 percent (e.g., 82 percent). In this case, the limiting crack length would be depicted in Figure 5-11 by the intersection of a horizontal line at $1.35x1.4\Delta P_{SLB}$ level with the solid line (through-wall burst line) which would put it at close to 0.44-inch. If the above is an accurate interpretation of the data in Figures 5-10 and 5-11, it would appear the statement at the bottom of the page 5-20: "When the

ligament tearing pressure is less than the 100 percent through-wall burst pressure, there can be a mixed mode pressure reduction up to 15 percent for circumferential average depths ≤80 percent" should be modified to either "reduction up to 35 percent" or to "for circumferential average depths ≤ 40 percent."

As a result of the above, please clarify the data in Figures 5-10 and 5-11. This clarification should address the maximum reduction in burst pressure for an axial flaw interacting with a circumferential flaw.

Response to Question B.3

As noted in the last paragraph of Section 5.5.2 (page 5-19) of WCAP-15573, Revision 1, the results for the 100 percent throughwall 0.24 inch and 0.48 inch electro discharge machining (EDM) notches were obtained by testing with a bladder (no foil), and represent incipient tearing results rather than burst. Upon incipient tearing, the bladder tends to extrude into a small opening leading to a bladder failure prior to burst of the indication. Bladder extrusion is common in testing throughwall EDM notches without a foil. These older test results were obtained from WCAP-15579, "Burst Pressure Data for Steam Generator Tubes with Combined Axial and Circumferential Cracks," dated August 2000, documenting tests performed in the 1990 time frame and were included for completeness of the data, but should not be used as burst pressure information.

As noted in Section 5.7 (page 5-22) of WCAP-15573, Revision 1, an axial throughwall length of about 0.25 inch is expected to encompass the potential throughwall indications satisfying burst and leakage requirements. The burst pressure reduction for a 0.24 inch throughwall axial indication intersecting a circumferential indication of about 73 percent average depth was found to be 9 percent (square data point in Figure 5-10 of WCAP-15573, Revision 1). The probability of a longer throughwall indication (> 0.25 inch) intersecting a circumferential indication near 80 percent depth would be even less than the probability estimates of Table 7-1 of WCAP-15573, Revision 1.

The 15 percent reduction in burst pressure at 80 percent average circumferential depth is based upon the test results for the 0.60 inch long, 79 percent depth notches as indicative of expected results when the ligament tearing pressure is less than the throughwall burst pressure. The intent of Figure 5-11 of WCAP-15573, Revision 1, is to identify the crack range (nominal properties) for which a 15 percent reduction could reduce the burst pressure below 1.4 times the steam line break primary to secondary differential pressure ($1.4\Delta P_{SLB}$) for indications that satisfy the burst margin requirement as isolated axial cracks. In plotting the figure, the 15 percent reduction is applied to the axial throughwall burst pressure as the burst pressure is defined as the larger of the ligament tearing or throughwall burst pressure. For the Figure 5-11 example, throughwall lengths less than 0.53 inch would have burst pressures more than 15 percent above $1.4\Delta P_{SLB}$ and the indications would satisfy the burst margin assuming a 15 percent reduction in the burst pressure.

The question addresses the potential reduction in the burst pressure for a 0.48 inch, 82 percent depth indication for which the ligament tearing pressure is approximately $1.4\Delta P_{SLB}$. For mixed mode effects, this flaw size is very similar to the test condition of 0.60 inch, 79 percent for which the ligament tearing pressure is also close to $1.4\Delta P_{SLB}$. Both indications have the ligament tearing pressure less than the burst pressure for a throughwall indication of the same length. The reduction in burst pressure for the 0.48 inch indication would be expected to be less than that for the 0.60 inch test condition since mixed mode effects tend to increase with length of the axial indication. Clearly, it is not appropriate to prepare a Figure like 5-11 based on assuming a large burst pressure reduction for a throughwall indication. The 15 percent reduction used to prepare Figure 5-11 is based on the mixed mode effects for a 0.53 inch indication being bounded by the 0.60 inch test results of a 15 percent reduction.

The 15 percent reduction is applicable to partial depth axial indications, and is a smaller reduction than obtained for long intersecting throughwall axial indications (e.g., for an intersecting 80 percent circumferential indication, the reduction for a 0.60 inch, 79 percent axial is 15 percent while the reduction is about 25 percent to 30 percent for a 0.60 inch throughwall axial - WCAP-15573, Revision 1, Figure 5-10 data). The 15 percent reduction for partial depth indications also envelops the reduction for a 0.24 inch throughwall indication, which bounds the expected range of EOC throughwall lengths under the ARC. The probability of finding a longer throughwall that also intersects an 80 percent deep circumferential indication is negligibly small. The WCAP-15573, Revision 1, statement (Section 5.5.3, page 5-20) related to the 15 percent reduction in burst pressure for a throughwall crack was intended to apply to the partial depth indications for which Figure 5-11 is constructed. It was not intended to apply to an intersecting throughwall indication, and the statement is, in retrospect, misleading. The WCAP-15573, Revision 1, position on throughwall indications is more correctly stated by the last sentence of the previous paragraph on page 5-20, the 15 percent reduction bounds throughwall indications of about 0.24 inch which would envelope most throughwall indications under the ARC that satisfy burst margin requirements.

It is concluded that WCAP-15573, Revision 1, does not require any modifications. The summary table of Section 5.7 notes that the 10 percent to 15 percent burst pressure reductions apply to partial depth cracks and up to about 0.25 inch throughwall cracks. Larger reductions could occur for intersecting throughwall lengths longer than 0.25 inch but the probability of this combination is too low for consideration in the ARC.

Question B.4

In paragraph 5.5.4 of WCAP-15573 revision 1 (page 5-20), a crack area adjustment factor of 1.4 and a leak rate adjustment factor of 1.7 (at 2560 pounds per square inch (psi)) were derived for a 0.6-inch long axial through-wall flaw if it intersected a 75 percent through-wall circumferential flaw. In Section 6.6.1, the assumption is made that these factors are upper bounds for all axial cracks <0.6-inch long interacting with a 50 to 80 percent through-wall circumferential flaw. Please provide the basis for this assumption (i.e., that the crack area and leak rate adjustment factors for a 0.6-inch long axial flaw is greater than the crack area and leak rate adjustment factor for smaller flaws). For example, how do we know that the area adjustment factor for a 0.5-inch long axial through-wall flaw intersecting an 80 percent deep circumferential flaw is ≤ 1.4?

Response to Question B.4

Figure 6-13 of WCAP-15573, Revision 1, illustrates the morphology concept employed for predicting the crack opening area for intersecting throughwall cracks. The presence of the circumferential crack is considered to release the tip of the axial crack so that it behaves as though the length were doubled. This is illustrative of the concept that the effect on the area of longer lengths is greater than the effect on shorter cracks. Figure 6 enclosed in this letter illustrates the crack opening area (COA) ratios calculated by the Zahoor model delineated in the Electric Power Research Institute (EPRI) Ductile Fracture Handbook. The COA is effectively an exponential function of the crack length. The imposition of a circumferential crack at the tip of an axial crack increases the flexibility of the material at the crack tip and leads to an attendant increase in the size of the plastic zone. It is standard practice to treat the COA as being dependent on the effective length of the crack, where the effective length is determined as a function of the size of the plastic zone. Figure 6 illustrates the results from considering effective total crack length increases of 1 percent and 5 percent. In both cases the COA ratio is an increasing function of the crack length. Hence, it is expected that the effect of a circumferential crack on the COA will increase with crack length and the use of a ratio derived from data for a 0.6 inch long crack will be conservative for shorter cracks.

Question B.5

Leak rate tests have been performed by the Office of Nuclear Regulatory Research. Prediction of the actual leak rates from these tests has led to mixed results. For EDM notches, predictions of actual leak rates using single phase flow (no flashing) orifice discharge equation are reasonable down to leak rates of few tenths of gpm. Similarly, predictions of actual leak rates for stress corrosion cracks, which are accompanied by a ligament rupture event and subsequent sudden increase of leak rate from essentially zero, are also reasonable. However, there are a number of cases where deeper cracks (approximately ≥ 80 percent average depth) occasionally leak in a gradually increasing manner with increasing pressure starting from pressures that are significantly lower than the predicted ligament rupture pressure. The leak rate predictions in these cases

are not as accurate. Most of these tests also showed time-dependent increase of leak rate at constant pressure hold. As a result of the above, please address the following: Discuss how the tests listed in Table 6-1 of WCAP-15573, Revision 1, behaved during leak rate tests, specifically, whether they experienced sudden ligament rupture prior to onset of leakage or started to leak from the start of the tests. Discuss the method used to calculate the through-wall crack lengths of these tests in order to predict the leak rate. Discuss whether the leak rate model assumed (or predicted) flashing within the tube wall for all the tests listed in Table 6-1. Also, discuss whether any measurements or Finite Element Analyses (FEA) on EDM notches were conducted to validate the crack opening area equation used in section 6.2.1.

Response to Question B.5

The data used in the development of the regression equation relating measured leak rate to estimated leak rate using the CRACKFLO code were from several different sources as identified in Table 6-1 of WCAP-15573, Revision 1. Multiple techniques and/or equipment were involved for testing and measuring the leak rate depending on when the tests were performed (techniques are judged to improve with time) and whether or not the tubes were laboratory or steam generator (radioactive) specimens. Data source number 2 specimens were fatigue grown cracks and are not susceptible to a time dependent increase in the flow unless material creep were to occur at the tips of the cracks. This would not be expected at the test temperature of interest.

Testing of pulled tube specimens, sources 3 and 6, was performed in hot cells at the Westinghouse Science and Technology Center. The procedure duration for measuring the leak rate was a function of the leak rate itself. For large leak rates, the capacity of the system would limit the duration of the test and replicate measurements were made to verify the initial readings. The number of replicates was determined by the test engineer at the time of the test. If the leak rate was low, repeat tests would be made over a period of about twenty to thirty minutes. The water was cooled, condensed, and captured in a graduated cylinder. The accumulated volume of water would be linear over time for a steady-state leak rate. Testing continued until at least two successive measurements were the same. For very slow leaks, the leak rate was measured by counting the number of drops that were condensed over a similar length of time. In all cases, the tests were repeated to verify the leak rate. Therefore, a minimum test period of 40 minutes would be typical of source 3 and 6 specimens. A similar procedure would have been used for laboratory generated PWSCC and outside diameter stress corrosion cracking cracks in source 1, 4 and 5 specimens.

It is believed that sudden ligament ruptures were not reported for any of the tests listed (sources 1 through 6). Some tests showed no leakage at normal operating conditions but did leak at SLB conditions. Therefore, it is likely that some ligament tearing was associated with the increase in pressure.

Figures 7 through 10 enclosed in this letter were used by Argonne National Laboratory (ANL) at the Steam Generator Workshop held by the NRC in Bethesda, Maryland, in

February of 2001, to illustrate the time dependent nature of the leak rate in some specimens. Not all specimens exhibited a time dependent leak rate. Figures 7 through 10 show the pressure and leak rate as a function of time for several specimens. Specimen SGL 177 was tested at ambient temperature. A small initial leak rate of 0.06 gpm was observed about 100 to 150 minutes after achieving a steady state pressure of 2500 psi. The time delay of 150 minutes after the pressure increase for the leak to increase from zero to 0.06 gpm is unusual in leak testing. The leak rate stayed constant until the pressure was raised again approximately 1000 minutes later. Specimen SGL 219 was tested at 540°F. The leak rate suddenly increased about 8 minutes after achieving a pressure of 2400 psi while showing no increase in leakage with increasing pressure until the step increase after 8 minutes. Specimen W2-10 (a doped steam specimen supplied by Westinghouse) did not achieve a steady state leak rate, but did exhibit a sudden jump in the leak rate about 300 minutes after the differential pressure was increased from 2500 psi to 2700 psi. The jump in the leak rate closely coincided with a change in the test from a room temperature test to a test at 282°C. The lower material properties at the higher temperature may have permitted a ligament to tear with the associated increase in the leak rate. Specimen SGL 822 likewise did not reach a steady state leak rate at constant pressure. The leak rate steadily increased from near zero to 5 gpm after a pressure of 2500 psi was reached. Except for the 150 minute delay for increased leakage in specimen SGL 177, the methods for conducting the tests performed by Westinghouse would have been sufficient to identify the increasing leak rate of the other ANL specimens because they did not achieve a steady state leak rate for a significant length of time. The behavior of SGL 177 is difficult to explain because it was tested at ambient conditions where no time dependent behavior would be expected, but the leakage did not occur until about 150 minutes after the increase in pressure to 2500 psi. Most of the increases in leak rate follow increases in the pressure differential across the tube, although there is a modest time delay is some cases. Since leak rate tests generally show direct increases in leakage with increases in pressure, these tests are unusual in the time delay for the leakage increase. The leak rate increases appear to be consistent with tearing a ligament following a pressure increase as opposed to increasing leak rates at constant pressure.

Throughwall crack lengths were not calculated, but were measured during the destructive examination of the specimens. The lengths represent corrosion throughwall lengths and would not include any ligament tearing that may have occurred during the leak rate testing.

The CRACKFLO model code for predicting the leak rates does include an internal determination of whether or not flashing is expected to occur within the crack. If the result is positive, then the backpressure that would be associated with flashing is accounted for. Since the predictions using CRACKFLO were scaled to test data results by the use of the regression relation of Table 6-4 in WCAP-15573, Revision 1, the magnitude of the prediction error standard deviation is likely increased if no flashing actually occurs. This latter situation had been reported as being the case from recent testing performed by ANL. Since the prediction error standard deviation would be

expected to increase if no flashing occurred, leak rate predictions of actual cracks with flashing would likewise be expected to be conservative.

Figures 11 and 12 enclosed in this letter provide a comparison of the stress intensity and area functions presented in section 6.2.1 of WCAP-15573, Revision 1, and in the EPRI Ductile Fracture Handbook (Zahoor). The figures demonstrate that the formulations are effectively identical in the range of interest, i.e., the half-length $\lambda \leq 5$. The EPRI formulations have been verified by ANL for estimating crack opening areas. There is a small difference in the use of the equations; WCAP-15573, Revision 1, reports that the flow stress is used for the determination of the plastic zone correction factor, while the EPRI formulation uses the yield stress. During development of the CRACKFLO code, comparisons were made of the Tada & Paris crack opening areas with test data. Regardless, predictions using the Tada & Paris equations via CRACKFLO have been scaled to the test data by the use of the regression relation of Table 6-4 of WCAP-15573, Revision 1, and any errors in the CRACKFLO models are encompassed in the uncertainties derived from the regression analysis with leak rate measurements.

Questions Related to NDE Issues

Question C.1

For mixed mode indications, the separation distance is basically being determined by counting the number of null points. In the axial direction, the number of null points is set by the rotating probe pitch and is fixed by probe rotational speed (i.e., revolutions per minute) and the push/pull speed. The number of null points along the circumferential direction is dependent on the digitization rate. Discuss whether over-sampling of data in the circumferential direction will lead to inaccurate null point evaluations. If so, discuss what procedures are in place for data acquisition personnel to preclude over-sampling of the data in the circumferential direction.

Response to Question C.1

For mixed mode indications, separation requirements are satisfied by meeting null point distance requirements as described in Section 4.8.5 of WCAP 15573, Revision 1. In the axial direction, the number of null points can be used in determining the null point distance although the null point distance could also be directly measured once the axial scale has been set. In the circumferential direction, the number of null points does not apply and the null distance must be measured such as by measuring the arc length for the null distance given the tube diameter.

The separation distance in the circumferential direction is not dependent on the sampling rate. The sampling rate and revolutions per minute determine the number of data points per revolution, which is a data quality parameter that does not determine the null distance.

Approved plant procedures govern how these distances are measured with eddy current data to insure that the measurements are consistently and correctly performed each outage.

Question C.2

It is stated that "The NDE circumferential crack sizing uncertainties of this report are intended to support mixed mode and tube integrity evaluations, and are not planned to support the tube repair decisions or an ARC. All detected circumferential cracks will be repaired." In lieu of this intention, it is not clear why there would be a need for a detailed profiling of circumferential indications using the proposed voltage-based sizing method. Please clarify.

Response to Question C.2

The efforts supporting profiling of circumferential indications were undertaken to provide sizing of the cracks found in an inspection to support mixed mode evaluations. For example, the WCAP-15573, Revision 1, supports acceptably small mixed mode effects for average circumferential depths < 80 percent. Circumferential indications at dented tube support plate intersections must be sized to support the expected condition of average depths < 80 percent. Conditional requirements on the leakage evaluations, as described in Section 7.9.5 of WCAP-15573, Revision 1, are dependent on the circumferential depths. Profiling of the circumferential indications is needed for the mixed mode assessments and for assessing the need to implement the conditional requirements. All detected circumferential cracks are repaired. The circumferential sizing efforts are not intended to justify leaving circumferential cracks in service.

Question C.3

In the sizing procedure for circumferential cracks based on the empirically developed exponential voltage response model, the threshold for adjusting the maximum depth to 100 percent is set at 7.0 volts. The phase-based sizing procedure for axial cracks, on the other hand, sets signals greater than 4.5 volts to 100 percent through-wall. Please discuss the basis for the difference in threshold values between the two procedures.

Response to Question C.3

The selection of 7.0 volts for the circumferential throughwall threshold was based on data for explosive expansions given in Figures 18a, 18b, 19a, and 19b in Enclosure 2 to this letter. Figures 18a, 18b, 19a, and 19b are reproduced from Figures G-14 and G-15 of Appendix G of EPRI Report TR-107197-P2, "Depth Based Structural Analysis Methods for SG Circumferential Indications," dated December 1997. EPRI Report TR-107197-P2 is a licensed product. The circumferential data show a greater spread in the non-throughwall and throughwall voltages than found for axial PWSCC such that selection of a threshold for circumferential cracks was not as well defined as for axial PWSCC. The 7.0 volts threshold was judgmentally selected to represent a value near

the middle of the circumferential throughwall voltages that also exceeded all non-throughwall voltages.

Reviews of similar data for axial PWSCC found a more well-defined distinction that nearly all throughwall indications were above about 4.5 volts and nearly all non-throughwall indications were less than 4.5 volts.

Question 3.1 from WCAP-15573, Revision 0, and Question 3.1 as Modified by NRC Question on February 6, 2002

Original Question 3.1

The Cochet/ASME model (used for condition monitoring) was shown to provide conservative estimates of the burst pressure of dented specimens. Since the ANL/EPRI model is generally less conservative than the Cochet/ASME model and was not developed with dented tube specimens, please confirm that the ANL/EPRI model gives realistic predictions for dented tubes.

Response to Original Question 3.1

The response to this question was provided in PG&E Letter DCL-02-019, "Response to NRC Request for Additional Information Regarding Supplement 3 to License Amendment Request 00-06, "Alternate Repair Criteria for Axial PWSCC at Dented Intersections in Steam Generator Tubing,'" dated February 26, 2002.

Question 3.1 as Modified by NRC Staff on February 6, 2002

Condition monitoring is based on the Cochet/ASME model. Figure 5.2 of WCAP-15573, Revision 1, depicts that this composite model is conservative based on the actual burst pressure (i.e., model predicted burst pressure is less than the actual burst pressure for nearly all cases). Similarly, Figure 5.3 of WCAP-15573, Revision 1, depicts that the normalized burst pressure is conservative. Equations 5-8 and 5-9 of WCAP-15573, Revision 1, are the normalized Cochet and ASME models, respectively. The "weak-link" (also referred to as the limiting equivalent rectangular crack) method is used in conjunction with Equations 5-8 and 5-9 to determine the lowest burst pressure of an indication (which is the higher value of either the Cochet or the ASME model for the limiting crack). This process yields the model predicted normalized burst pressure. The model predictions are still conservative.

With the model predicted normalized burst pressures, equation 5-10 of WCAP-15573, Revision 1, is then used to obtain the "revised" model predicted normalized burst pressures which are plotted against the "measured" normalized burst pressures in Figure 5-4 of WCAP-15573, Revision 1. Note that the conservatism of the model prediction that was apparent in Figure 5-3 has disappeared in Figure 5-4 because of

the regression fit. If the model was "good" on the average, the model predicted normalized burst pressures would scatter randomly about the "measured" normalized burst pressures, (i.e., all the symbols in Figure 5-3 would scatter randomly above and below the 45 degree perfect fit line). Since they don't, the model has a systematic bias and it is this bias that makes the model predictions conservative in Figure 5-3. Equation 5-10 is used to correct for the model error (i.e., remove the bias) and the "revised" model normalized burst pressures are no longer uniformly conservative. Figure 5-4 depicts this relationship. The uncertainty in the model predictions is now represented by the scatter about the perfect fit line. Figures 5-5 and 5-6 of WCAP-15573, Revision 1, show that the errors in the (log) predictions are randomly scattered about the zero line and that the residuals of log (pressures) are normally distributed. In the Monte Carlo simulations for condition monitoring, the mean burst pressure is predicted first (using Equations 5-8, 5-9, 5-10) and then a random error based on this distribution is added. Note that this random error results from both model uncertainty and uncertainties due to other effects such as use of the equivalent rectangular approach, presence of dents, etc.

For the operational assessment (OA), the ANL/EPRI model is used along with the mp uncertainties (model error) developed for rectangular EDM slots. Since the ANL/EPRI model is more accurate, the figure corresponding to Figure 5-3 may show less or no systematic bias in the predicted pressures and the range of scatter about the perfect fit line may be less than that in Figure 5-4. If there was no systematic bias, a correction like Equation 5-10 is not needed. In the Monte Carlo analysis for OA, the mean burst pressure is predicted first using ANL/EPRI model and then an error is added based on the distribution of error in mp which was derived from tests on EDM notches. Additional uncertainties due to the use of the equivalent rectangular crack approach or the presence of dents are not included, like what was done for the condition monitoring assessment. As a result, the error in the OA may be underestimated.

This was the basis for the RAI question regarding using the test data from Figure 5-2 and plotting them against the ANL/EPRI predictions and use the same approach as with Cochet/ASME to estimate the error.

The previous question assumes that the test data in Figure 5-2 are not corrupted; however, Equation 5-10 is based on measured data that may have been influenced by the tube pressurization rate. That is, the measured normalized burst pressure may be artificially high. To summarize, there appears to be another component of uncertainty that is not addressed under the proposed operational assessment methodology, namely the ability of the ANL model to predict the burst pressure of a dented tube specimen with stress corrosion cracking using the weak link methodology. The assumption under the current proposal appears to be that the uncertainty in the model developed by ANL using notches is the same as the uncertainty for a stress corrosion crack modeled as an equivalent rectangular crack. The basis for this assumption has not been provided.

Response to Question 3.1 as Modified by NRC Staff on February 6, 2002

During a telephone conference call held on February 5, 2002, between PG&E personnel, Westinghouse personnel, representatives from the NRC staff, and representatives from ANL, it was requested that a figure similar to Figure 5-2 of WCAP-15573, Revision 1, be prepared using the ANL model. Since the ANL model was developed specifically for predicting ligament tearing, the pressure resisting capability of a tube with a throughwall crack is calculated to be zero. Therefore, to use the model for burst prediction, as is done for operational assessments, the ANL model must be used in conjunction with the EPRI throughwall burst prediction model. As noted in the NRC discussion it is to be expected that the ANL/EPRI model predictions will more closely approximate the measured data. This is because it is known that ANL model predictions may be higher than the Cochet model predictions. For example, for the specimen data used to develop the ANL model, a comparison of ANL and Cochet predictions is provided on Figure 13 enclosed in this letter.

All of the analyses of the tested specimens were repeated using the ANL/EPRI model in response to the NRC request. For reference purposes, a recreation of Figure 5-2 of WCAP-15573, Revision 1, is provided as Figure 14 enclosed in this letter. The results of the analyses using the ANL/EPRI model are illustrated on Figure 15 enclosed in this letter. The measured burst pressures tend to exceed the predicted burst pressures when the prediction is above about 4000 psi. To further gauge the performance of the model in the operational assessment results, a plot of the measured pressures versus the lower 5th percentile predictions is provided on Figure 16 enclosed in this letter. This information illustrates that the ANL model may be expected to lead to a conservative prediction of the burst pressure for a variety of cracked tube specimens when the weak link methodology is employed. The level of conservatism appears to diminish when the predicted burst pressures are less than about 4000 psi although the predictions remain generally conservative.

In addition to examining the effect of using the ANL/EPRI model, an evaluation was made of specimens for which it was judged to be unlikely that a foil reinforced bladder would have been used. It is normal practice to reinforce the crack location of the specimen with a lubricated bladder and piece of brass foil if it is judged likely that the radial ligament will tear and result in a pressure loss before bursting of the specimen is achieved. A reasonable rule-of-thumb for the judgment is that the maximum depth is suspected of being greater than about 85 percent of the tube thickness. A plot of the measured burst pressure versus the predicted burst pressure, for specimens where the maximum depth from the destructive examination (DE) was found to be greater than 85 percent (foil likely) and less than 85 percent (foil unlikely), is shown on Figure 17 enclosed in this letter. The use of the maximum DE depth is considered sufficient for this evaluation. For practical purposes there does not appear to be any difference in the results.

Table 4-7R1. Diablo Canyon Axial PWSCC Growth Rate Data Through 2R10 Outages									
						Adjusted NDE Growth/EFPY - DCCP at 603 °F			
Outage	SG	Row	Column	Location	Crack No.	Length (in.)	Max. Depth (%)	Avg. Depth (%)	Max. Volts
1R8	1	17	39	01H	1	-0.09	-25.58	-18.37	0.37
1R8	1	21	42	01H	1	0.02	-15.89	-9.82	0.20
1R8	1	21	44	01H	1	-0.02	4.65	3.39	0.28
1R8	1	18	64	01H	1	0.05	0.78	2.08	0.54
1R8	1	18	64	03H	1	0.01	1.55	1.25	0.29
1R8	2	26	43	02H	1	-0.06	-9.30	0.10	0.17
1R8	2	43	49	03H	1	-0.01	-2.58	-1.05	0.26
1R8	2	35	56	02H	1	-0.07	0.00	-0.77	0.34
1R8	2	5	66	02H	1	0.02	-14.73	-4.98	0.36
1R8	2	35	67	03H	1	0.02	-19.38	-7.27	0.39
1R8	2	7	68	03H	1	-0.02	8.53	8.17	0.19
1R8	2	14	72	02H	1	0.04	-10.85	-8.15	0.23
1R8	2	16	73	01H	1	0.00	-3.10	-1.07	0.28
1R8	2	14	74	01H	1	-0.04	-8.53	-7.05	0.40
1R8	2	35	77	01H	1	-0.02	23.26	12.85	0.30
1R8	2	35	77	01H	2	-0.01	-25.58	-16.36	0.55
1R8	2	13	81	01H	1	0.00	-23.64	-20.30	0.32
1R8	2	16	82	01H	1	-0.05	5.04	7.09	0.06
1R8	3	32	47	03H	1	0.04	-7.75	-4.08	0.65
1R8	4	38	27	01H	1	0.00	-9.30	-4.36	0.55
1R8	4	39	58	01H	1	0.00	-18.99	-11.33	0.32
2R8	2	2	2	01H	1	-0.02	13.58	10.01	-0.01
2R8	2	14	15	01H	1	0.06	1.85	2.89	0.19
2R8	2	19	15	01H	1	0.02	3.09	4.20	0.01
2R8	2	18	16	01H	1	0.04	0.93	3.93	0.18
2R8	2	6	24	01H	1	0.02	1.85	0.15	0.09
2R8	2	4	28	01H	1	0.05	1.85	2.11	0.18
2R8	2	12	28	01H	1	0.02	11.73	12.50	0.25
2R8	2	14	29	01H	1	0.01	0.00	-2.64	0.06
2R8	2	17	36	01H	1	0.02	-19.75	-13.48	0.14
2R8	2	15	42	01H	1	0.00	0.00	1.98	0.04
2R8	2	18	44	01H	1	0.02	8.64	5.40	0.11
2R8	2	22	45	01H	1	0.02	0.00	0.81	0.15
2R8	4	34	34	01H	1	0.02	7.41	4.88	0.07
2R8	4	4	37	01H	1	-0.01	9.26	4.01	0.19
1R9	1	9	6	01H	1	-0.01	11.73	7.97	-0.08
1R9	1	22	7	03H	1	0.04	8.64	6.17	0.31
1R9	1	23	14	03H	1	0.04	8.64	4.77	0.11
1R9	1	19	15	03H	1	0.07	0.00	-3.41	0.07
1R9	1	24	20	02H	1	-0.01	4.94	3.40	0.07

Table 4-7R1. Diablo Canyon Axial PWSCC Growth Rate Data Through 2R10 Outages									
						Adjusted NDE Growth/EFPY - DCCP at 603 °F			
Outage	SG	Row	Column	Location	Crack No.	Length (in.)	Max. Depth (%)	Avg. Depth (%)	Max. Volts
1R9	1	30	21	02H	1	0.05	-2.47	-2.50	0.01
1R9	1	34	24	03H	1	0.05	0.00	0.22	0.03
1R9	1	20	33	01H	1	0.02	1.54	-0.41	0.01
1R9	1	38	42	03H	1	0.05	3.40	0.89	0.04
1R9	1	22	71	02H	1	-0.01	4.63	5.42	0.06
1R9	2	17	9	06H	1	-0.01	17.90	9.54	-0.01
1R9	2	15	10	01H	1	0.02	-15.43	-3.76	0.06
1R9	2	11	27	01H	1	0.03	12.65	12.32	0.10
1R9	2	26	39	02H	1	0.05	5.86	4.21	0.08
1R9	2	11	45	01H	1	0.01	1.23	-0.10	0.01
1R9	2	6	47	01H	1	0.02	3.70	2.08	0.05
1R9	2	11	47	02H	1	0.01	0.00	-3.07	0.04
1R9	2	20	48	03H	1	-0.04	-7.41	-1.76	0.07
1R9	2	27	50	01H	1	0.00	8.02	5.48	0.17
1R9	2	35	52	03H	1	0.12	3.09	1.64	0.17
1R9	2	7	53	03H	1	-0.07	10.49	8.53	0.03
1R9	2	25	55	02H	1	0.02	3.70	1.73	0.09
1R9	2	16	57	01H	1	0.05	4.94	-1.28	0.20
1R9	2	38	66	01H	1	0.02	1.23	3.83	0.09
1R9	2	33	68	02H	1	-0.14	8.64	5.31	0.02
1R9	2	4	69	01H	1	0.01	1.23	6.64	0.05
1R9	2	19	74	02H	1	0.01	0.62	-0.51	0.06
1R9	2	13	75	02H	1	0.01	0.00	-0.43	-0.02
1R9	2	5	77	05H	1	0.01	8.02	6.35	0.07
1R9	2	26	79	01H	1	0.04	8.02	8.62	0.12
1R9	2	8	80	02H	1	0.04	0.00	1.21	0.04
1R9	2	23	82	01H	1	0.00	6.48	4.92	0.00
1R9	2	5	84	01H	1	0.01	5.56	2.71	0.19
1R9	2	9	87	4H	1	-0.02	-8.02	-7.78	-0.01
1R9	2	8	90	03H	1	0.03	8.64	7.63	0.15
1R9	2	2	92	05H	1	0.02	0.00	-0.24	-0.06
1R9	4	17	24	01H	1	0.03	0.00	0.06	-0.02
1R9	4	20	25	01H	1	-0.02	0.00	1.84	-0.02
1R9	4	46	42	01H	1	0.01	3.70	3.93	-0.05
1R9	4	35	68	03H	1	-0.01	0.62	-0.20	0.12
1R9	4	21	76	01H	1	0.04	5.56	4.60	-0.05
2R9	2	6	3	01H	1	0.02	7.53	3.49	0.05
2R9	2	18	7	01H	1	0.08	10.96	8.09	0.23
2R9	2	5	21	01H	1	0.02	17.81	14.56	0.08
2R9	2	21	23	02H	1	-0.01	7.53	8.46	-0.04
2R9	2	8	26	01H	1	0.01	-10.62	-10.69	0.15
2R9	2	5	33	01H	1	0.00	0.00	0.45	0.12

Table 4-7R1. Diablo Canyon Axial PWSCC Growth Rate Data Through 2R10 Outages									
						Adjusted NDE Growth/EFPY - DCCP at 603 °F			
Outage	SG	Row	Column	Location	Crack No.	Length (in.)	Max. Depth (%)	Avg. Depth (%)	Max. Volts
2R9	2	28	38	01H	1	0.01	6.16	3.83	0.01
2R9	2	16	39	04H	1	-0.04	4.11	4.36	0.09
2R9	2	16	39	04H	2	-0.02	0.68	1.75	0.05
2R9	2	14	40	01H	1	0.02	-4.79	-0.16	0.36
2R9	2	21	40	01H	1	-0.04	2.74	5.64	0.07
2R9	2	22	46	01H	1	-0.01	-0.68	-0.13	0.08
2R9	3	21	78	03H	1	0.09	8.90	10.81	0.08
2R9	4	17	31	03H	1	-0.02	4.11	0.68	0.13
2R9	4	14	53	03H	1	-0.01	0.00	0.33	0.06
1R10	1	22	7	03H	1	0.07	6.71	3.04	0.25
1R10	1	23	14	03H	1	0.01	-4.70	-3.69	0.09
1R10	1	19	15	03H	1	0.03	0.67	0.43	0.09
1R10	1	15	16	02H	1	-0.03	0.67	1.94	0.09
1R10	1	24	20	02H	1	0.02	1.34	-5.35	0.00
1R10	1	30	21	02H	1	-0.05	0.00	-0.05	-0.04
1R10	1	22	23	02H	1	-0.01	2.68	3.86	-0.01
1R10	1	22	23	02H	2	0.00	0.00	4.63	0.05
1R10	1	34	24	03H	1	0.08	-4.70	0.75	0.05
1R10	1	3	28	02H	1	0.01	0.67	4.38	0.21
1R10	1	14	28	02H	1	0.00	-6.71	-5.61	0.11
1R10	1	36	30	02H	1	0.02	-0.67	1.41	0.34
1R10	1	20	33	01H	1	-0.01	-3.36	-0.06	-0.02
1R10	1	4	41	01H	1	0.08	10.07	10.05	0.08
1R10	1	24	67	02H	1	0.04	0.00	0.50	0.10
1R10	1	22	71	02H	1	0.07	1.34	-3.73	0.11
1R10	2	13	10	01H	1	0.01	2.68	1.71	0.17
1R10	2	15	10	01H	1	0.03	-6.71	-6.12	0.05
1R10	2	16	12	05H	1	0.01	0.67	3.89	-0.05
1R10	2	8	15	02H	1	0.01	4.03	1.66	0.14
1R10	2	14	16	04H	1	0.00	-3.36	-1.24	0.15
1R10	2	30	16	01H	1	-0.07	-8.72	-3.69	0.23
1R10	2	25	17	02H	1	0.08	-2.01	-2.72	0.14
1R10	2	23	25	03H	1	0.03	2.68	4.54	0.31
1R10	2	42	28	02H	1	-0.01	6.04	6.25	0.17
1R10	2	7	31	01H	1	0.05	-4.70	-5.33	0.13
1R10	2	19	31	04H	1	-0.05	0.67	-0.53	0.09
1R10	2	9	34	02H	1	-0.03	0.67	-1.22	0.11
1R10	2	33	37	01H	1	0.01	0.00	-0.58	0.08
1R10	2	26	39	02H	1	0.03	-0.67	-1.91	0.30
1R10	2	11	45	01H	1	0.04	8.72	3.57	0.26
1R10	2	14	45	01H	1	0.00	0.00	-0.11	0.02
1R10	2	20	48	03H	1	0.07	3.36	-0.99	0.15

Table 4-7R1. Diablo Canyon Axial PWSCC Growth Rate Data Through 2R10 Outages									
						Adjusted NDE Growth/EFPY - DCCP at 603 °F			
Outage	SG	Row	Column	Location	Crack No.	Length (in.)	Max. Depth (%)	Avg. Depth (%)	Max. Volts
1R10	2	27	50	01H	1	0.01	2.68	0.40	0.24
1R10	2	29	51	02H	1	0.07	-0.67	-3.39	0.20
1R10	2	34	51	06H	1	0.06	-0.67	0.03	0.15
1R10	2	35	52	03H	1	-0.01	-2.68	-0.83	0.13
1R10	2	23	54	01H	1	0.04	0.00	-0.06	0.05
1R10	2	25	55	02H	1	-0.01	-2.01	0.33	-0.08
1R10	2	9	56	01H	1	0.00	1.34	1.81	0.17
1R10	2	27	56	01H	1	0.02	0.00	1.34	0.15
1R10	2	4	57	01H	1	-0.02	0.00	-0.38	-0.01
1R10	2	36	60	04H	1	0.03	-2.68	-6.09	0.09
1R10	2	8	61	02H	1	0.05	-5.37	-2.02	0.21
1R10	2	8	61	02H	2	0.08	3.36	0.32	0.10
1R10	2	32	62	01H	1	0.06	6.71	7.11	0.01
1R10	2	41	62	01H	1	-0.05	4.70	4.21	0.09
1R10	2	38	63	01H	1	0.06	1.34	2.63	0.32
1R10	2	39	64	03H	1	0.00	5.37	5.97	0.11
1R10	2	28	66	02H	1	-0.01	-11.41	-7.59	0.09
1R10	2	38	66	01H	1	0.05	7.38	1.55	0.10
1R10	2	33	68	02H	1	0.03	-4.03	-4.31	0.05
1R10	2	4	69	01H	1	0.01	0.00	-1.23	0.08
1R10	2	27	71	01H	1	0.05	0.67	-1.67	0.12
1R10	2	6	74	03H	1	0.03	0.00	-1.22	0.06
1R10	2	19	74	02H	1	0.01	-4.03	3.03	0.05
1R10	2	25	74	01H	1	0.01	6.71	5.89	0.13
1R10	2	2	76	02H	1	0.04	0.00	-3.46	0.07
1R10	2	5	77	05H	1	0.04	2.01	1.13	0.12
1R10	2	24	77	01H	1	0.05	3.36	4.11	0.11
1R10	2	2	78	01H	1	-0.01	-2.01	0.66	0.27
1R10	2	31	78	05H	1	0.07	4.70	-1.40	0.11
1R10	2	26	79	01H	1	0.01	0.00	1.52	0.21
1R10	2	23	82	01H	1	0.03	3.36	2.52	0.03
1R10	2	13	84	01H	1	0.00	-8.05	-7.42	-0.11
1R10	2	13	84	01H	2	0.03	-2.01	-5.69	-0.23
1R10	2	2	92	05H	1	0.02	0.00	0.29	0.03
1R10	2	2	92	05H	2	0.01	0.00	-0.37	0.05
1R10	2	2	92	05H	3	0.05	0.00	-4.53	0.06
1R10	2	2	93	04H	1	0.02	-14.09	-13.69	0.00
1R10	2	8	93	01H	1	-0.03	-6.71	-4.50	0.10
1R10	4	17	24	01H	1	-0.03	0.00	0.95	0.01
1R10	4	20	25	01H	1	0.02	0.00	0.43	0.01
1R10	4	35	36	02H	1	0.01	0.00	1.09	-0.03
1R10	4	46	42	01H	1	0.13	0.67	-3.12	0.01

Table 4-7R1. Diablo Canyon Axial PWSCC Growth Rate Data Through 2R10 Outages									
						Adjusted NDE Growth/EFPY - DCCP at 603 °F			
Outage	SG	Row	Column	Location	Crack No.	Length (in.)	Max. Depth (%)	Avg. Depth (%)	Max. Volts
1R10	4	39	48	03H	1	0.01	0.00	0.42	-0.03
1R10	4	39	58	01H	1	0.11	0.00	-0.77	0.16
1R10	4	35	61	02H	1	0.01	1.34	5.16	0.07
1R10	4	35	68	03H	1	0.03	-2.01	0.27	-0.09
1R10	4	38	69	02H	1	0.02	5.37	8.42	0.05
1R10	4	21	70	03H	1	0.02	14.09	8.83	0.09
1R10	4	21	76	01H	1	-0.01	3.36	1.98	-0.03
1R10	4	21	84	01H	1	0.07	1.34	3.78	0.01
2R10	2	5	3	01H	1	0.12	8.33	4.41	-0.05
2R10	2	17	12	01H	1	0.02	6.94	4.85	0.33
2R10	2	14	15	02H	1	0.01	6.25	8.11	0.06
2R10	2	19	15	01H	1	0.02	0.00	0.45	0.02
2R10	2	11	19	01H	1	0.03	10.42	4.69	0.13
2R10	2	15	22	01H	1	0.03	7.64	3.79	0.14
2R10	2	2	23	01H	1	0.00	4.86	4.74	0.00
2R10	2	21	23	02H	1	0.03	8.33	7.22	0.06
2R10	2	27	23	01H	1	0.00	14.58	11.87	-0.03
2R10	2	6	24	01H	1	0.04	-3.47	-2.79	-0.04
2R10	2	13	25	03H	1	0.01	4.17	6.57	0.08
2R10	2	2	26	01H	1	0.01	13.19	11.62	0.03
2R10	2	5	26	01H	1	0.02	6.25	4.52	0.10
2R10	2	8	26	01H	1	0.01	18.75	15.74	-0.12
2R10	2	7	27	01H	1	0.05	-1.39	-2.13	0.03
2R10	2	4	28	01H	1	0.02	4.86	3.84	-0.10
2R10	2	6	31	01H	1	0.03	0.00	2.70	0.04
2R10	2	7	32	01H	1	0.01	6.25	3.05	0.09
2R10	2	9	32	01H	1	-0.02	0.69	0.87	-0.01
2R10	2	5	33	01H	1	0.05	11.81	8.28	-0.02
2R10	2	3	34	01H	1	-0.01	6.94	4.90	0.10
2R10	2	4	34	04H	1	0.01	0.00	-0.87	0.04
2R10	2	6	36	01H	1	0.03	7.64	6.36	-0.16
2R10	2	28	38	01H	1	0.01	0.00	-4.91	-0.01
2R10	2	12	39	01H	1	0.01	6.25	2.71	-0.17
2R10	2	16	39	04H	1	0.03	7.64	6.43	0.05
2R10	2	16	39	04H	2	0.01	11.11	6.88	0.03
2R10	2	21	40	01H	1	0.00	1.39	1.95	-0.01
2R10	2	13	41	01H	1	-0.02	8.33	6.55	-0.01
2R10	2	21	41	01H	1	0.03	-3.47	-1.71	0.01
2R10	2	15	42	01H	1	-0.02	-4.17	-2.42	-0.03
2R10	2	8	43	04H	1	0.00	7.64	5.64	0.01
2R10	2	22	44	04H	1	0.03	10.07	2.66	-0.01
2R10	2	25	44	05H	1	0.08	0.00	-0.03	-0.08

Table 4-7R1. Diablo Canyon Axial PWSCC Growth Rate Data Through 2R10 Outages									
						Adjusted NDE Growth/EFPY - DCCP at 603 °F			
Outage	SG	Row	Column	Location	Crack No.	Length (in.)	Max. Depth (%)	Avg. Depth (%)	Max. Volts
2R10	2	14	45	01H	1	0.03	0.00	-4.00	-0.06
2R10	2	22	45	01H	1	0.04	9.72	9.30	-0.06
2R10	2	16	49	01H	1	0.03	5.56	-0.50	-0.06
2R10	2	15	51	01H	1	0.01	-1.39	-2.45	-0.03
2R10	2	27	59	01H	1	0.06	16.67	19.26	0.17
2R10	3	45	56	01H	1	0.01	-5.56	-5.39	0.06
2R10	3	21	78	03H	1	0.02	-5.56	-3.98	0.03
2R10	4	16	11	03H	1	0.06	-6.94	-7.96	0.03
2R10	4	11	17	03H	1	0.04	2.78	0.28	-0.13
2R10	4	12	17	03H	1	0.01	2.08	2.00	0.10
2R10	4	14	53	03H	1	0.03	1.39	-0.96	0.05
				Average Growth		**0.017**	**1.41**	**1.23**	**0.09**
				95th Percentile		**0.074**	**11.73**	**9.54**	**0.33**
				Maximum Growth		**0.128**	**23.3**	**19.3**	**0.6**

Table 4-8R1. Diablo Canyon Axial PWSCC Depth, Length and Voltage Growth/EFPY Distributions							
Average Depth Combined Data from Cycles 1R9, 2R8, 2R9 and 2R10		**Maximum Depth** Combined Data from Cycles 1R9, 2R8, 2R9 and 2R10		**Length** Combined Data from Cycles 1R9, 1R10 and 2R10		**Maximum Volts** Combined Data from Cycles 1R9, 2R8, 2R9 and 2R10	
Growth/EFPY (%)	**CDF**	**Growth/EFPY (%)**	**CDF**	**Growth/EFPY (inch)**	**CDF**	**Growth/EFPY (volt)**	**CDF**
0.0	0.278	0.0	0.261	0.000	0.225	0.000	0.278
0.7	0.348	0.8	0.348	0.010	0.296	0.012	0.330
1.5	0.400	1.7	0.400	0.014	0.420	0.028	0.400
2.9	0.504	2.9	0.452	0.020	0.550	0.050	0.522
4.1	0.600	3.9	0.504	0.031	0.651	0.066	0.600
5.3	0.713	4.9	0.548	0.040	0.698	0.085	0.696
6.5	0.800	6.0	0.600	0.040	0.751	0.100	0.757
7.6	0.852	6.5	0.652	0.043	0.799	0.115	0.800
8.6	0.904	7.4	0.696	0.051	0.852	0.150	0.870
10.0	0.930	7.9	0.748	0.060	0.899	0.170	0.904
12.0	0.957	8.4	0.800	0.067	0.923	0.196	0.948
14.5	0.983	9.4	0.852	0.080	0.953	0.204	0.957
19.3	1.000	11.1	0.904	0.081	0.959	0.230	0.965
		11.7	0.922	0.100	0.976	0.300	0.983
		13.2	0.948	0.120	0.988	0.380	1.000
		15.0	0.965	0.140	1.000		
		20.0	1.000				

Figure 4-14R1

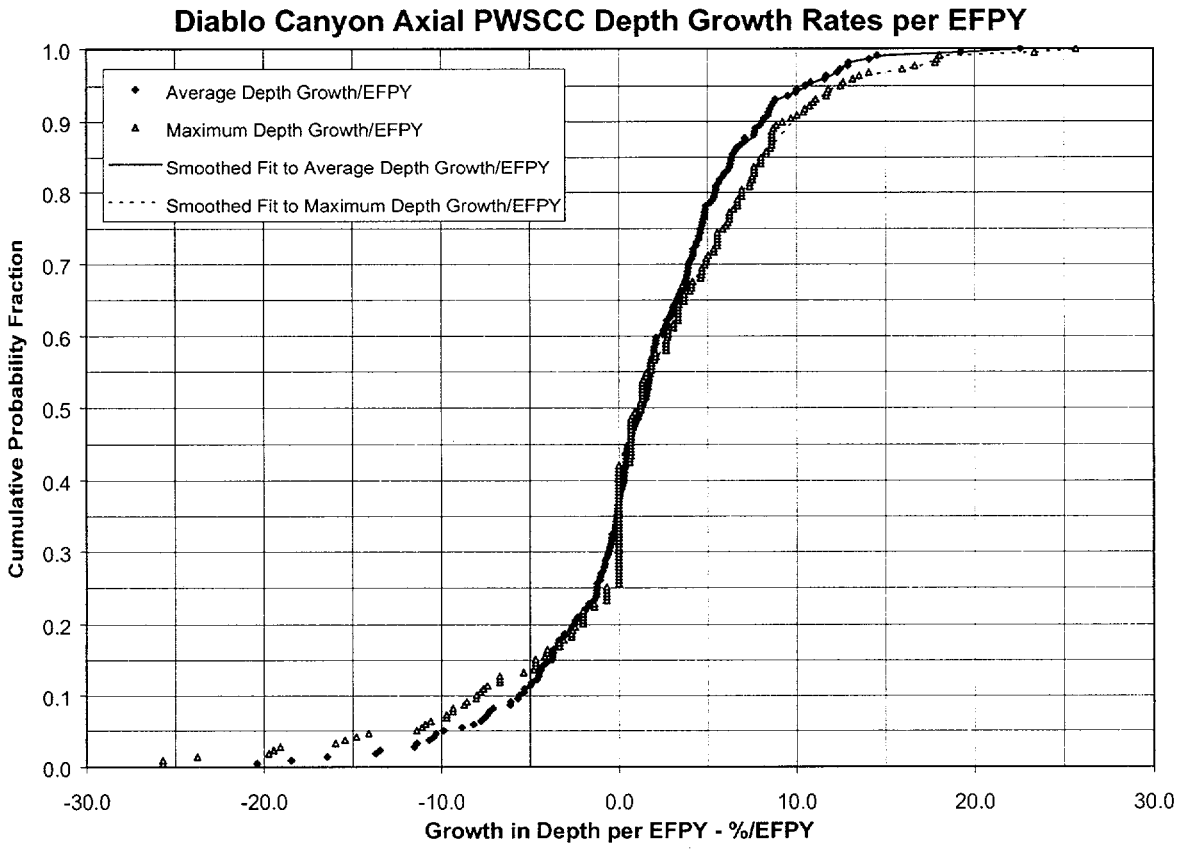

Figure 4-15R1

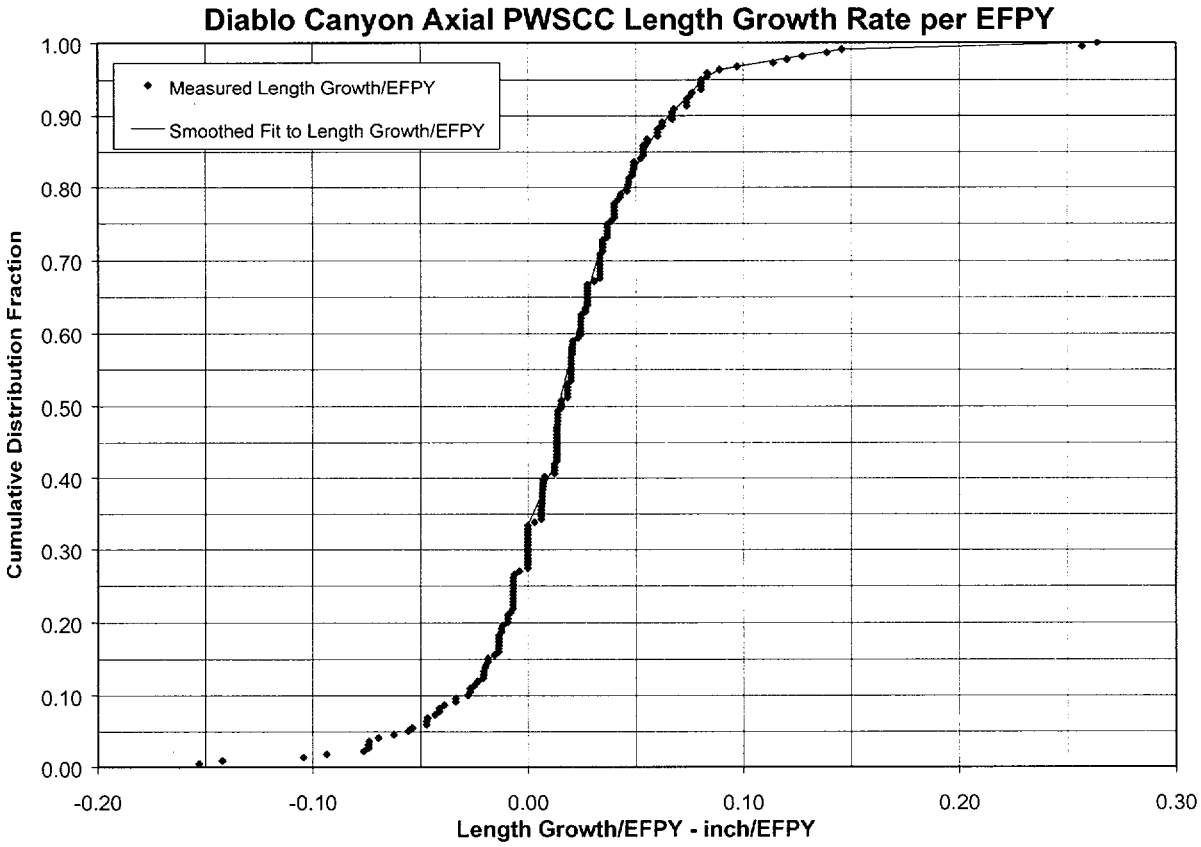

Figure 4-16R1

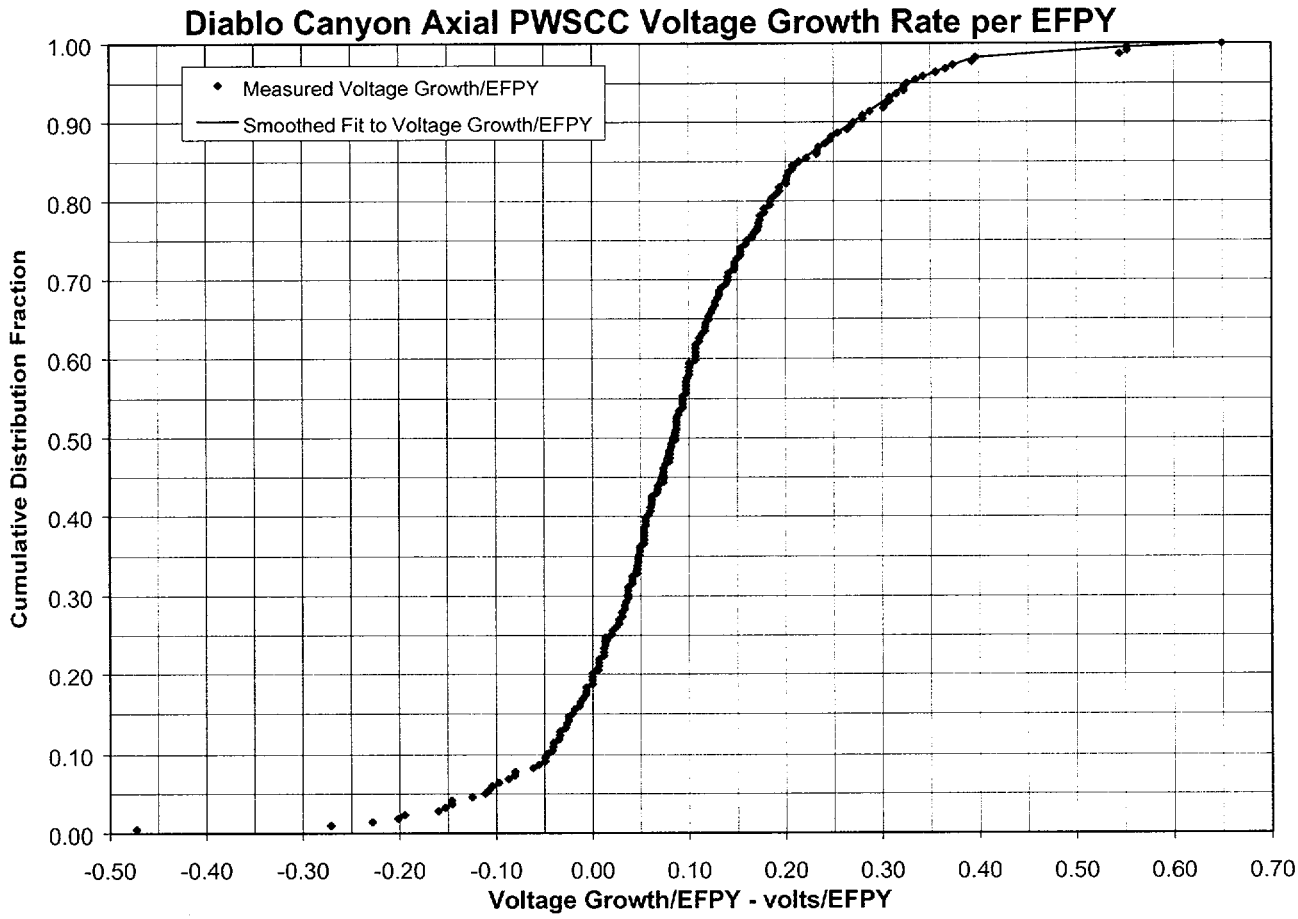

Figure 1

Diablo Canyon Average Depth Growth Data
Comparison of Cumulative Distributions Between Cycles

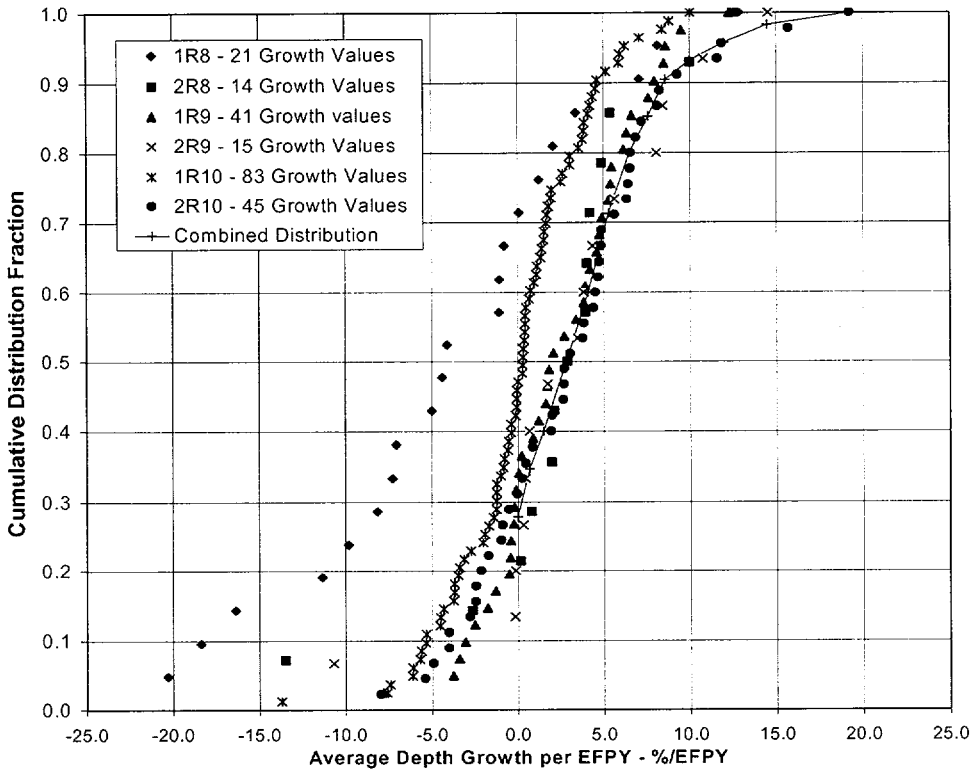

Figure 2

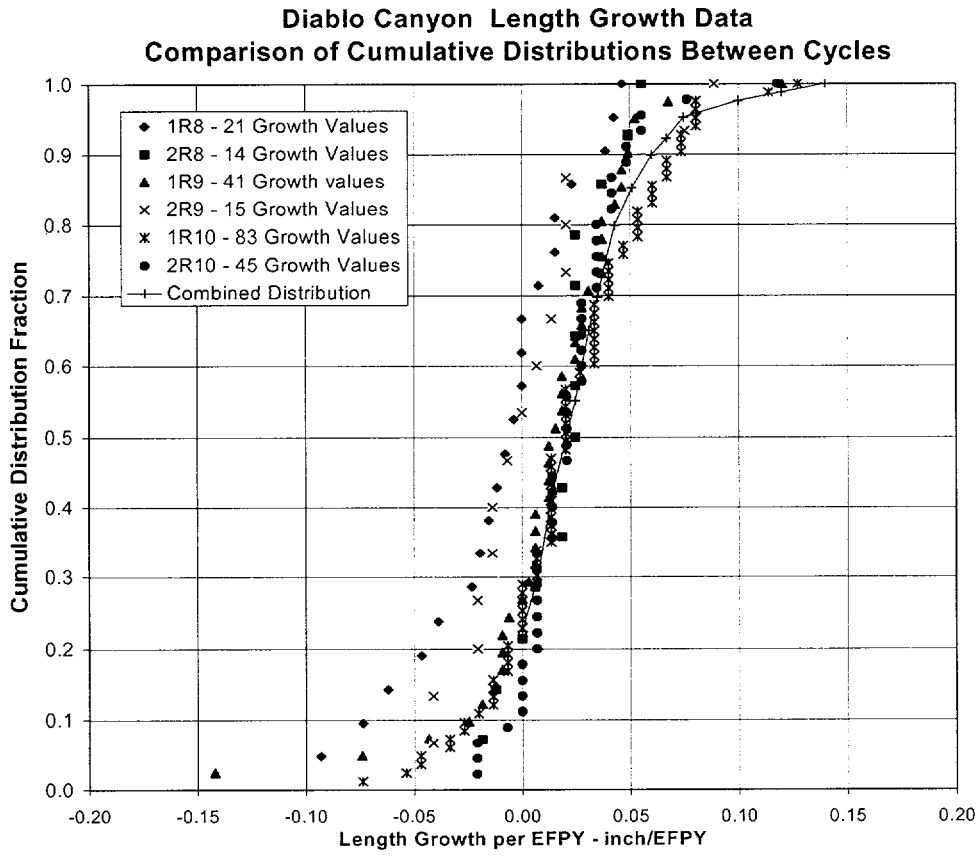
Diablo Canyon Length Growth Data
Comparison of Cumulative Distributions Between Cycles
1R8 - 21 Growth Values
2R8 - 14 Growth Values
1R9 - 41 Growth values
2R9 - 15 Growth Values
1R10 - 83 Growth Values
2R10 - 45 Growth Values
Combined Distribution
Cumulative Distribution Fraction
1.0
0.9
0.8
0.7
0.6
0.5
0.4
0.3
0.2
0.1
0.0
-0.20
-0.15
-0.10
-0.05
0.00
0.05
0.10
0.15
0.20
Length Growth per EFPY - inch/EFPY

Figure 3

Diablo Canyon Axial PWSCC: Average Depth Growth vs. BOC Depth

Combined Data for Cycles 2R8, 1R9, 2R9, 1R10 and 2R10

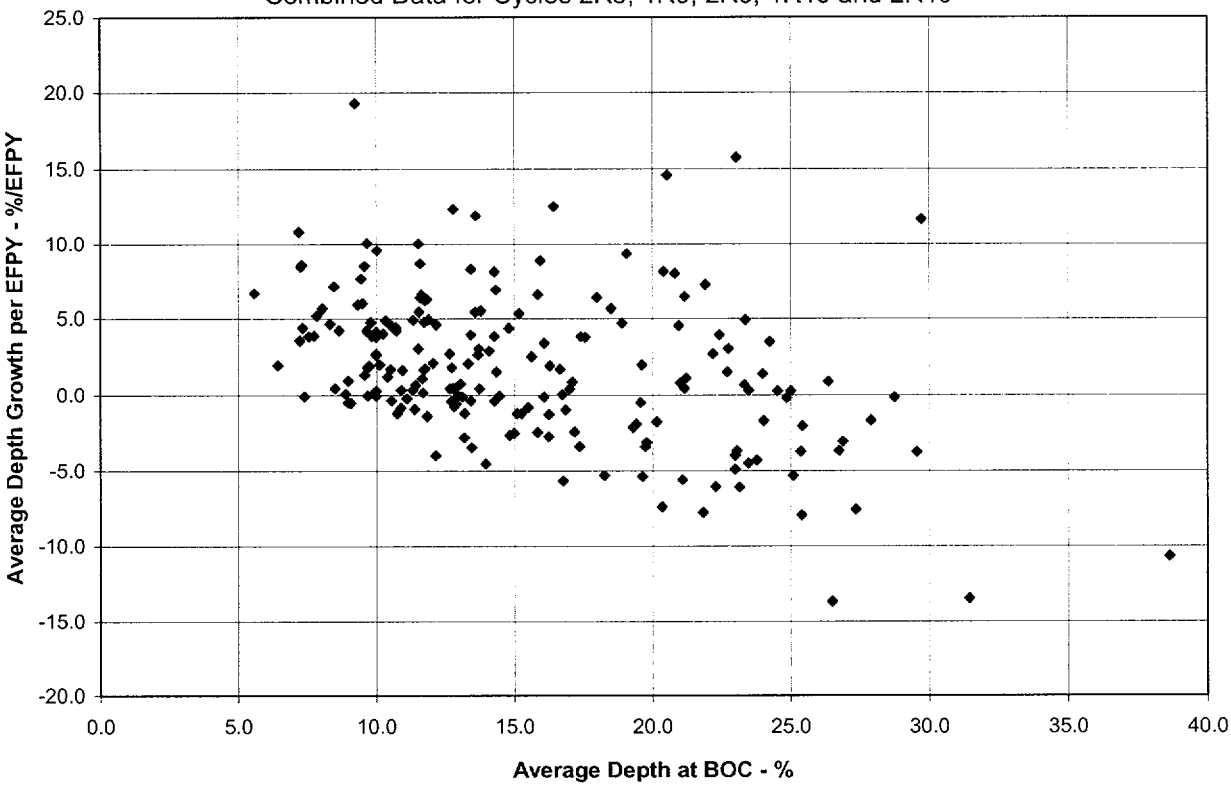

Figure 4

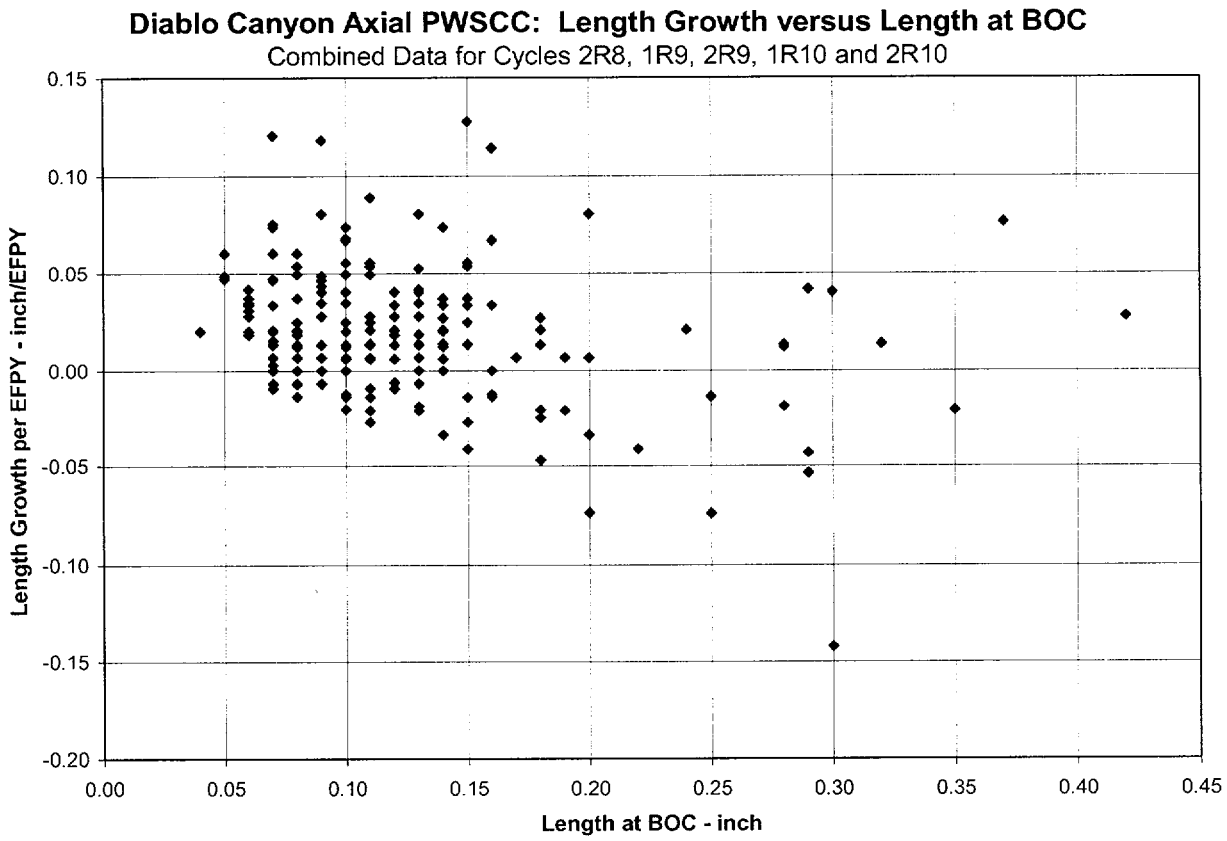
Diablo Canyon Axial PWSCC: Length Growth versus Length at BOC
Combined Data for Cycles 2R8, 1R9, 2R9, 1R10 and 2R10
Length Growth per EFPY - inch/EFPY
0.15
0.10
0.05
0.00
-0.05
-0.10
-0.15
-0.20
0.00
0.05
0.10
0.15
0.20
0.25
0.30
0.35
0.40
0.45
Length at BOC - inch

Figure 5

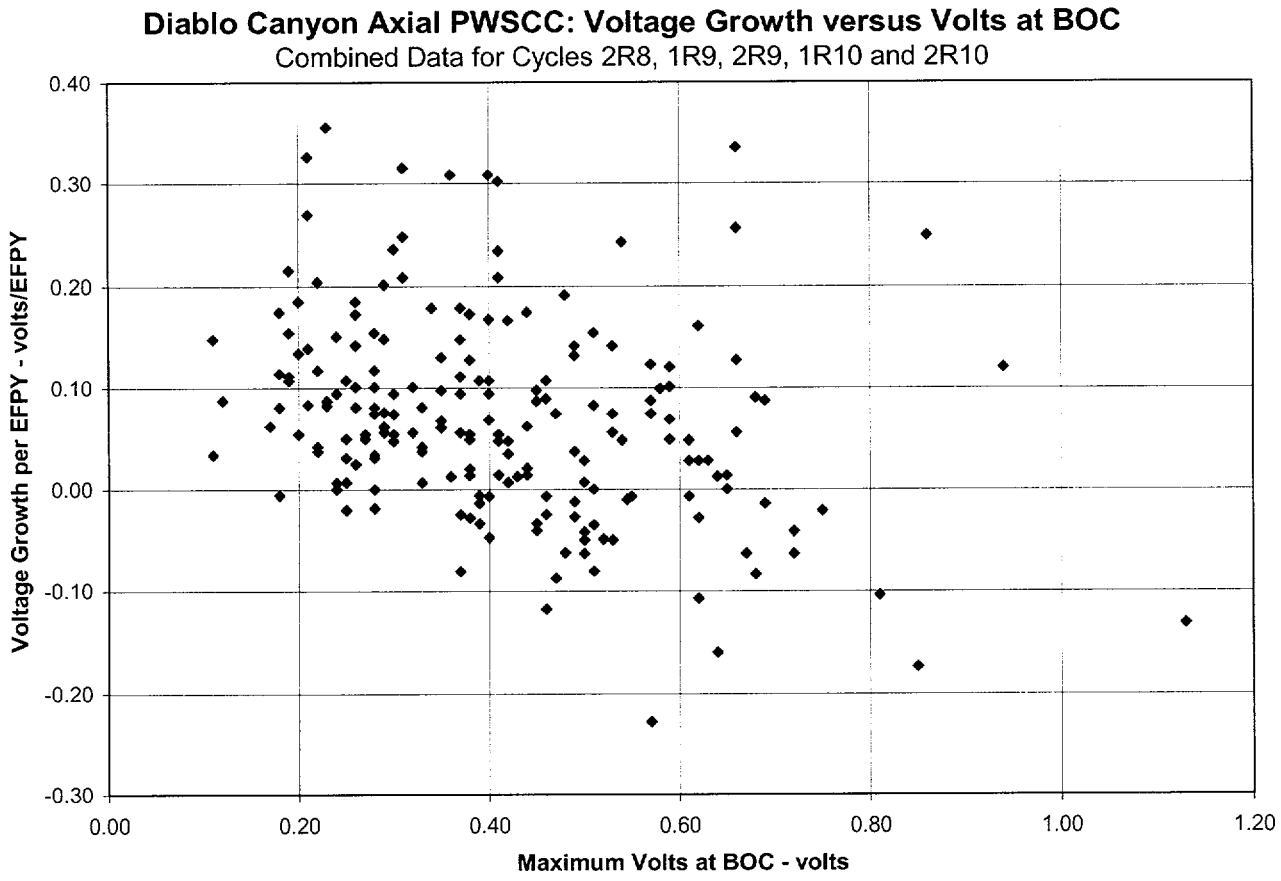
Diablo Canyon Axial PWSCC: Voltage Growth versus Volts at BOC
Combined Data for Cycles 2R8, 1R9, 2R9, 1R10 and 2R10
Voltage Growth per EFPY - volts/EFPY
0.40
0.30
0.20
0.10
0.00
-0.10
-0.20
-0.30
0.00
0.20
0.40
0.60
0.80
1.00
1.20
Maximum Volts at BOC - volts

Figure 6

Node Release Effect

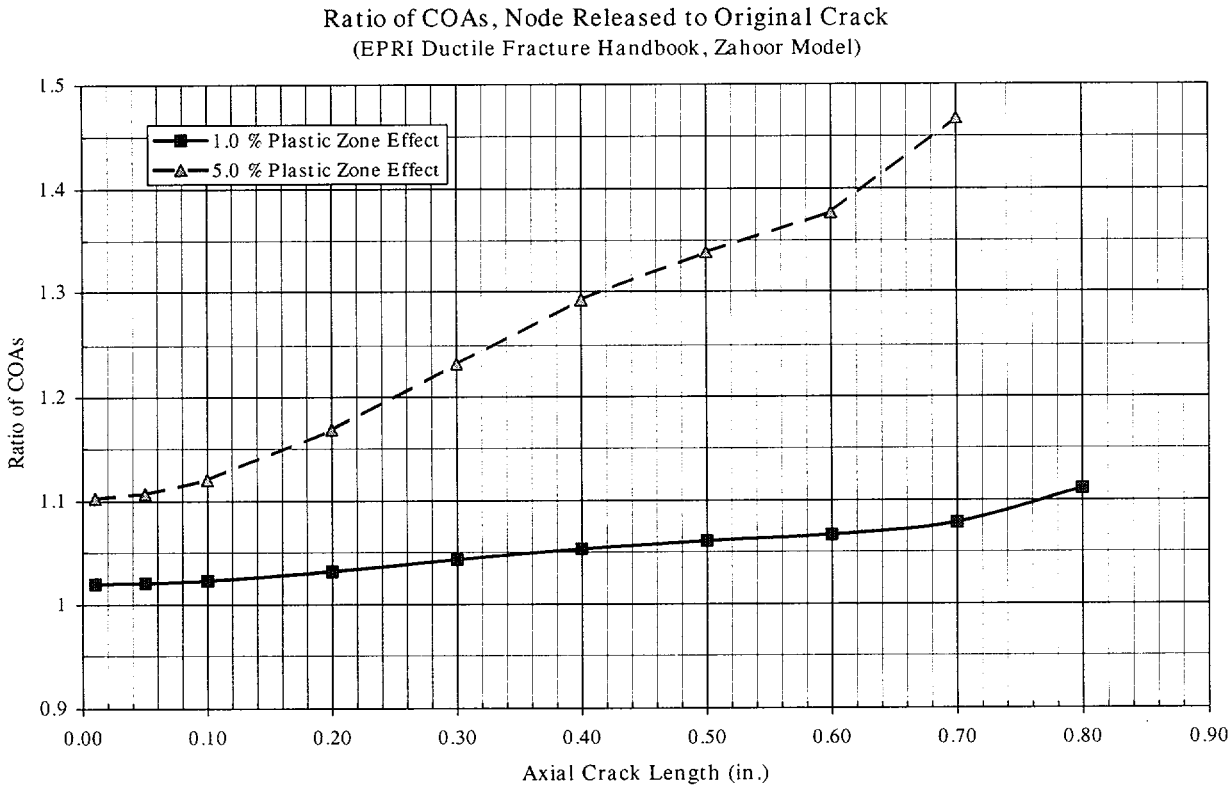

Figure 7

ANL Specimen Exhibiting Increase in Leak Rate with Time

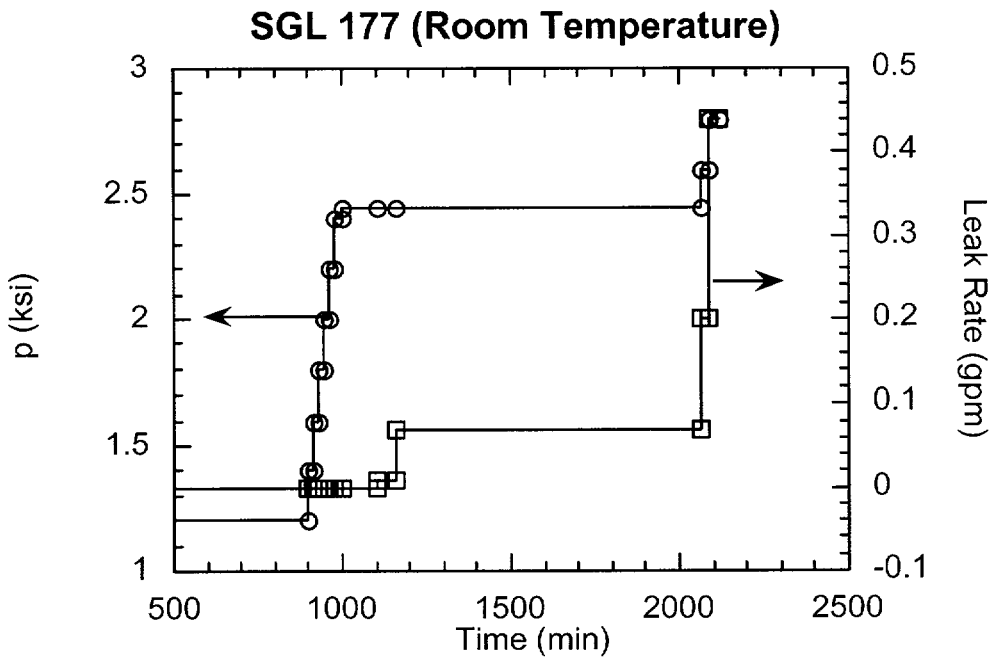

Figure 8

ANL Specimen Exhibiting Increase in Leak Rate with Time

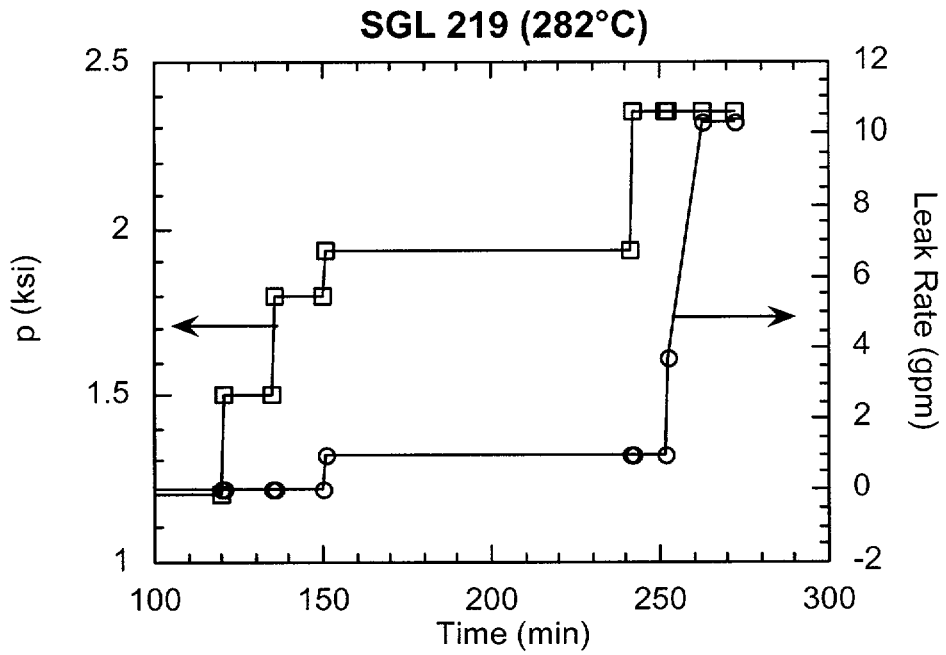

Figure 9

Westinghouse Supplied Specimen Exhibiting Increase in Leak Rate

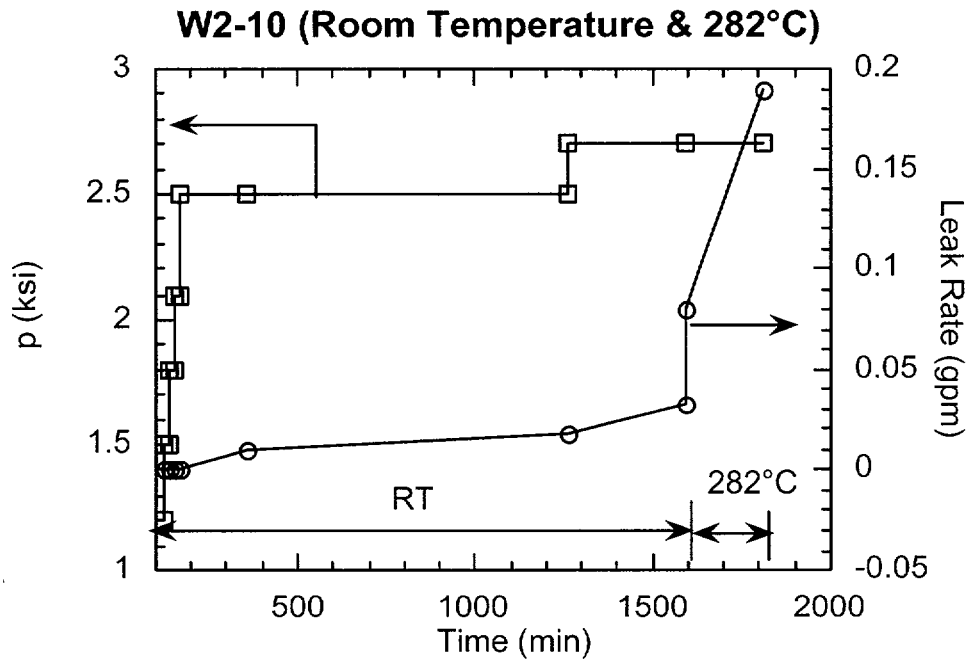

Figure 10

ANL Specimen Exhibiting Time Dependent Leak Rate

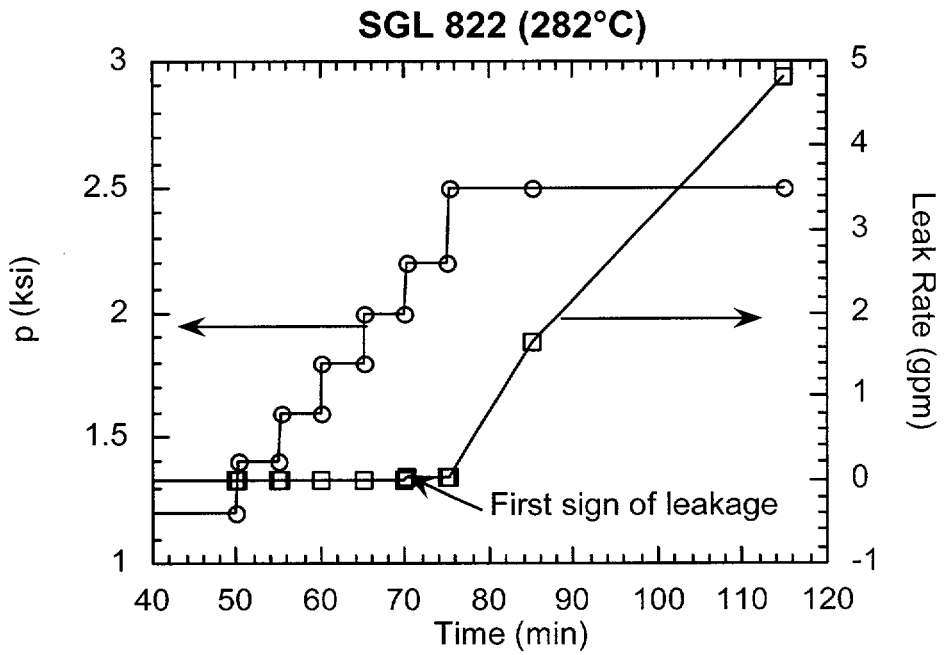

Figure 11

Comparison of Stress Intensity Factor Functions Developed by Paris & Tada With That of Zahoor

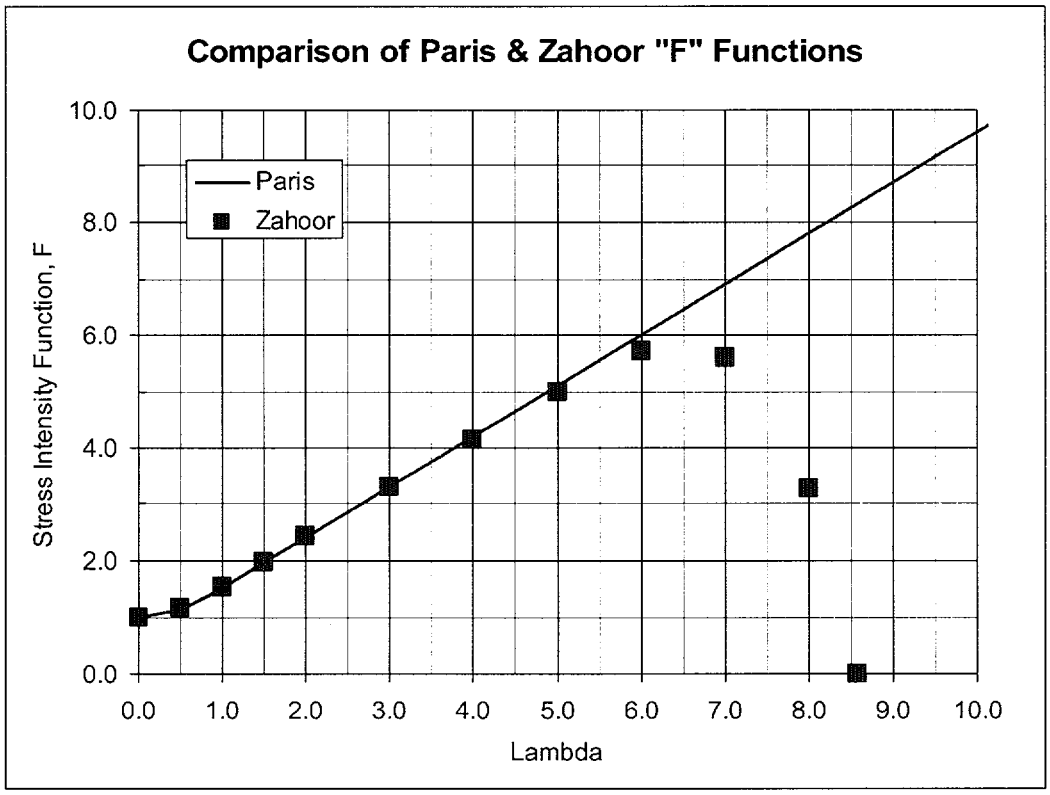

Figure 12

Comparison of Area Functions Developed By Tada & Paris With That of Zahoor

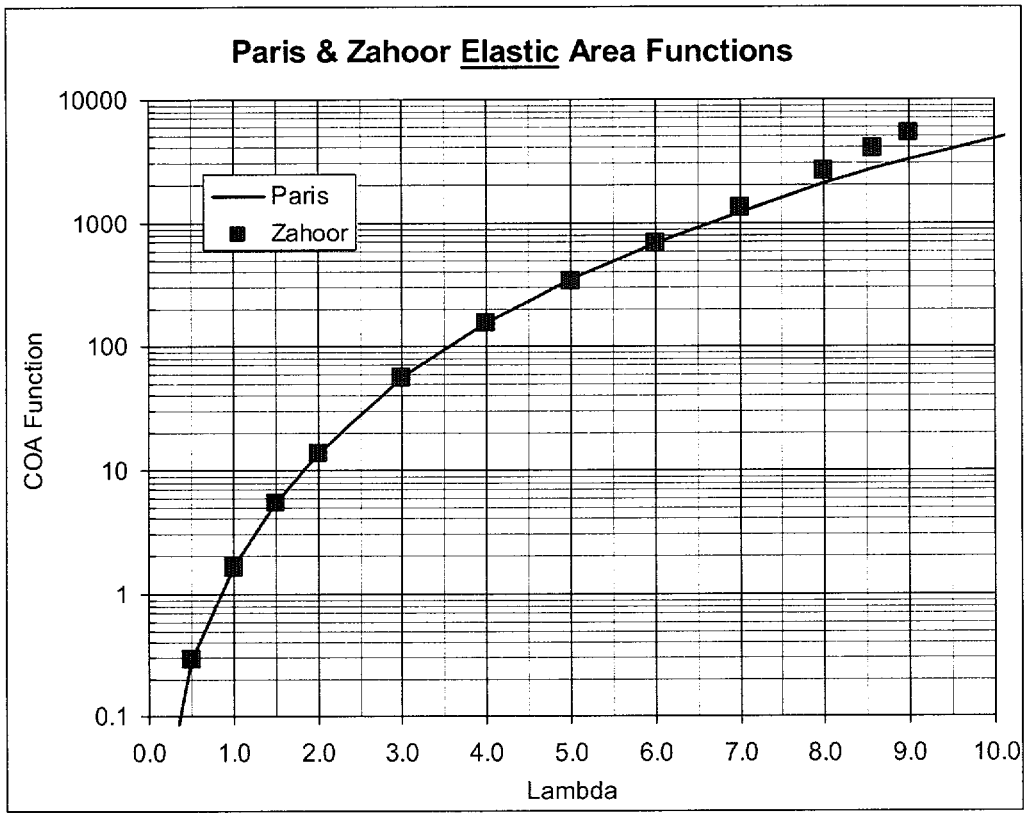

Figure 13

Cochet Versus ANL Model Predictions for PNL Data

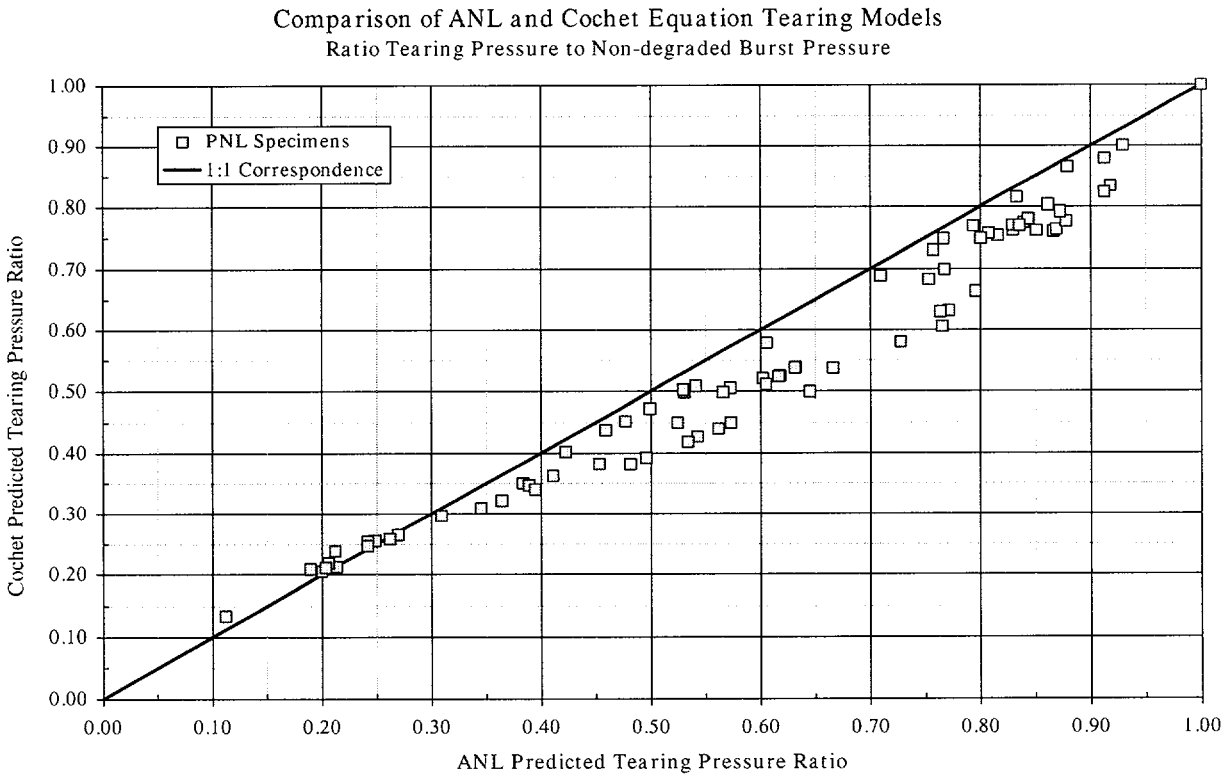

Figure 14

Reproduction of Figure 5-2 of WCAP-15573, Revision 1

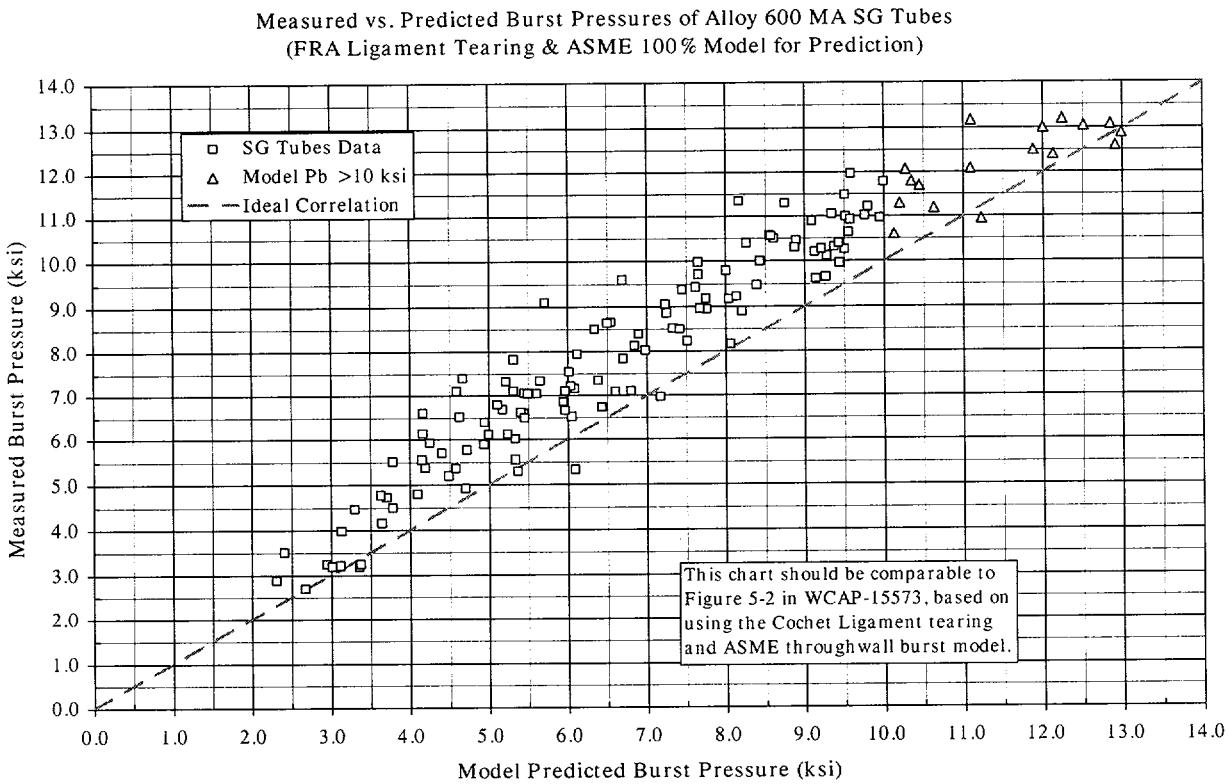

Figure 15

Results Obtained Using the ANL/EPRI Model for the Predictions

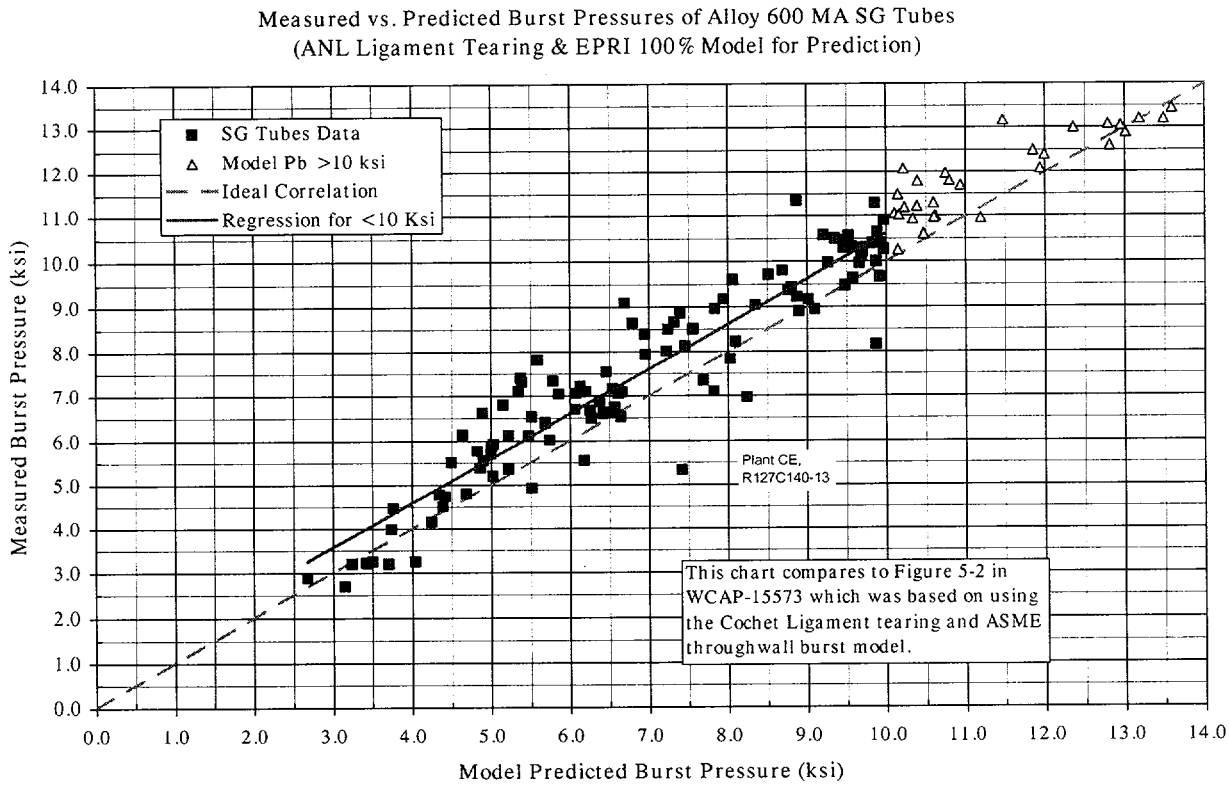

Figure 16

ANL/EPRI Model Lower 95th Percentile Predictions

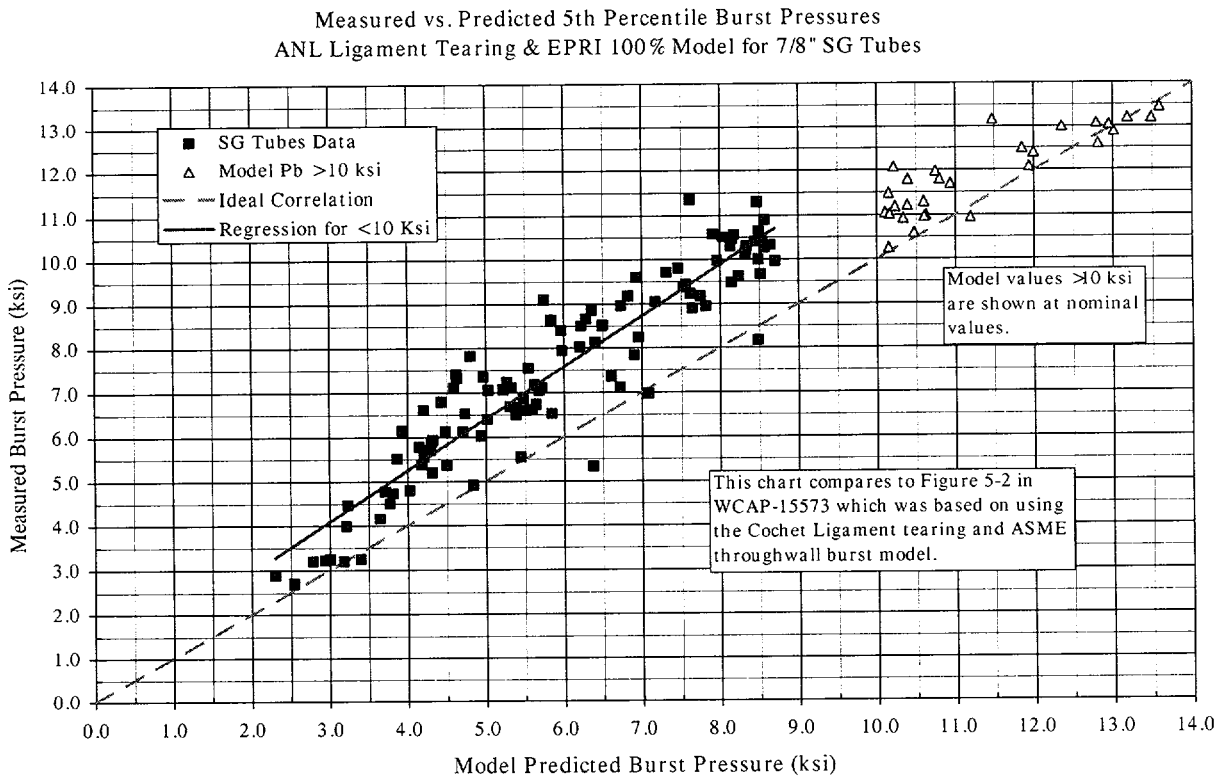

Figure 17

Cochet/ASME Model for Specimens < 85% and > 85% Maximum Depth

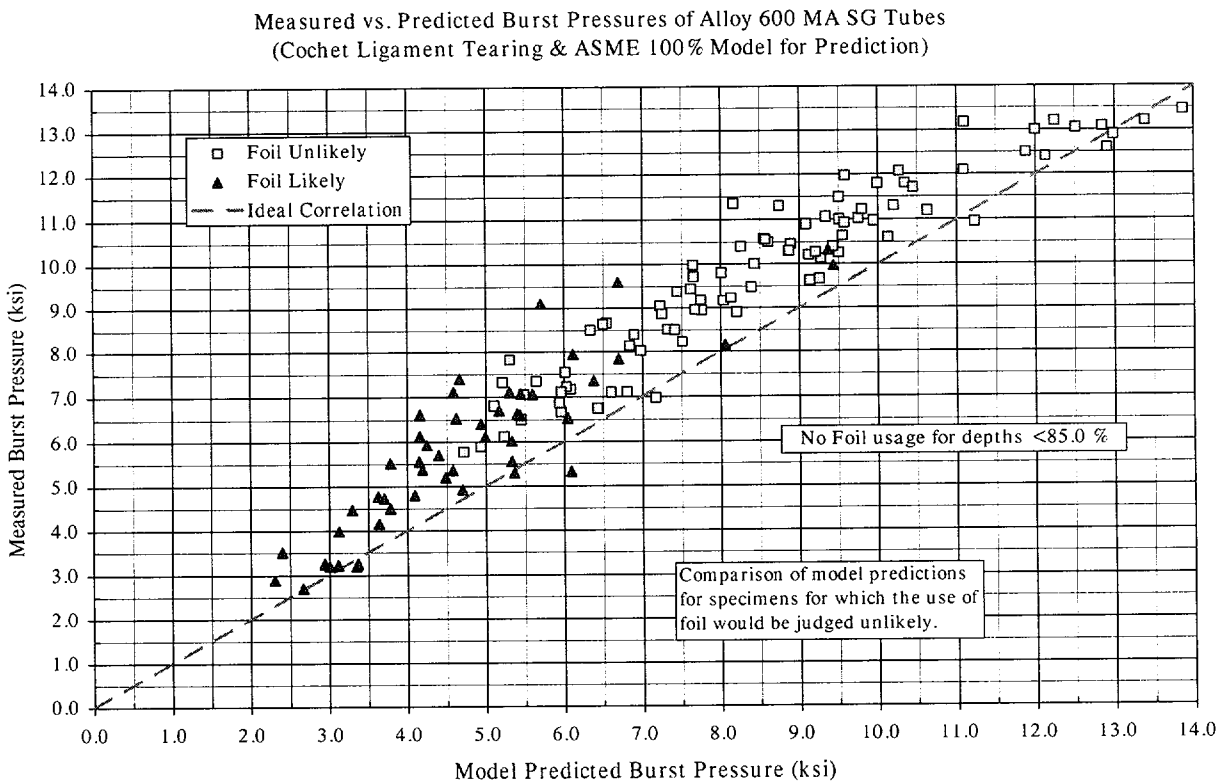

Data for Explosive Expansions Used to Determine Circumferential Throughwall Threshold

Figures 18a, 18b, 19a, 19b
(4 pages)

Reproduced from Figures G-14 and G-15 contained in Appendix G of Electric Power Research Institute (EPRI) Report TR-107197-P2, "Depth Based Structural Analysis Methods for SG Circumferential Indications," dated December 1997, an EPRI licensed product.

Figure 18a

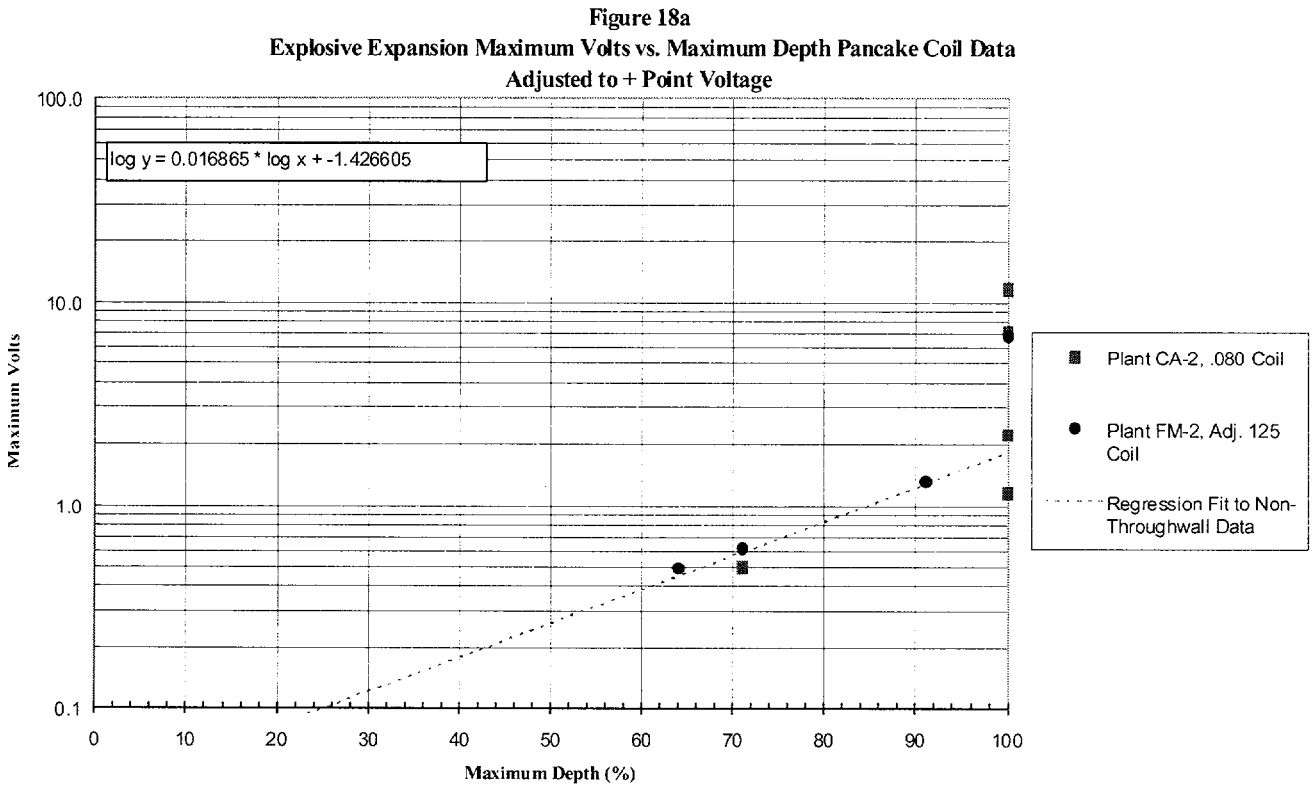

Reproduced from Figure G-14a contained in Appendix G of Electric Power Research Institute (EPRI) Report TR-107197-P2, "Depth Based Structural Analysis Methods for SG Circumferential Indications," dated December 1997, an EPRI licensed product.

Figure 18b

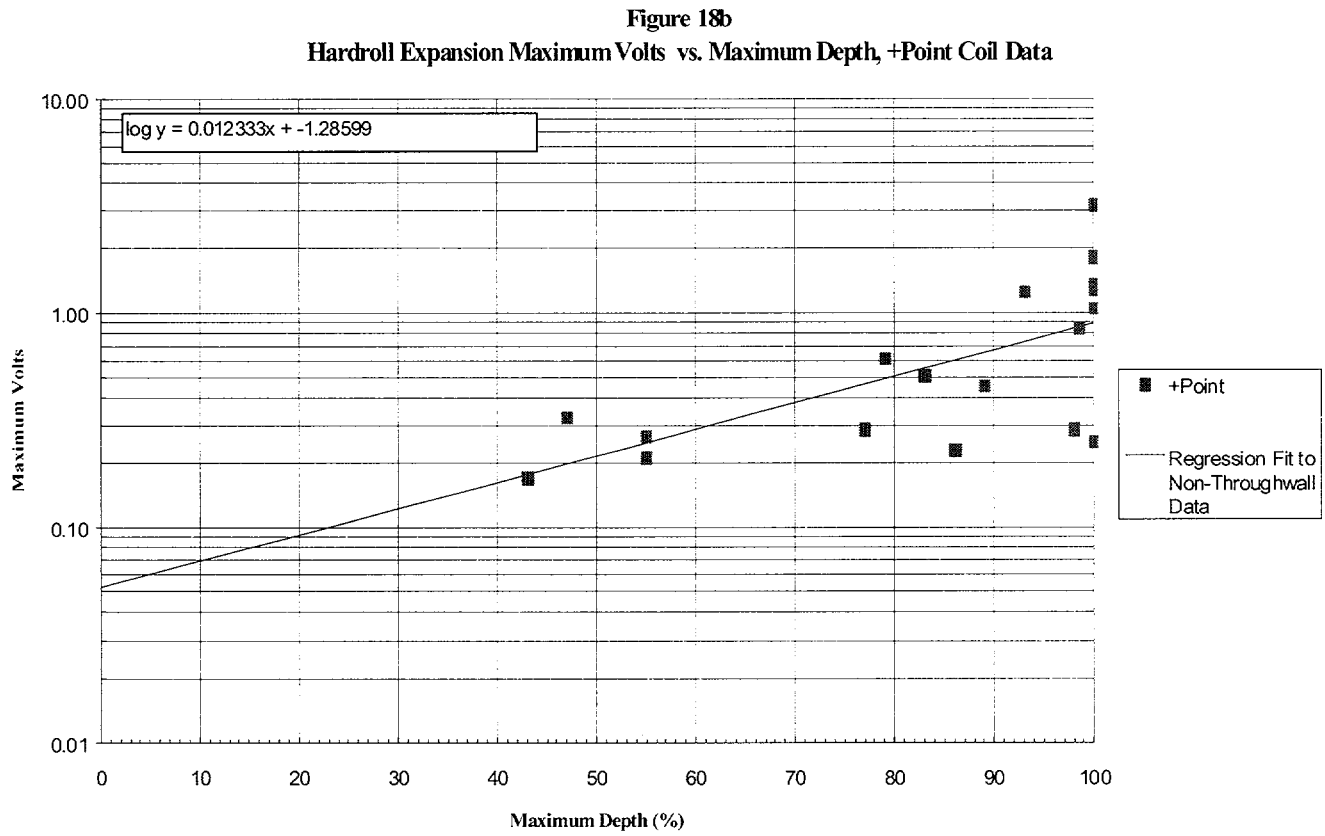

Reproduced from Figure G-14b contained in Appendix G of Electric Power Research Institute (EPRI) Report TR-107197-P2, "Depth Based Structural Analysis Methods for SG Circumferential Indications," dated December 1997, an EPRI licensed product.

Figure 19a

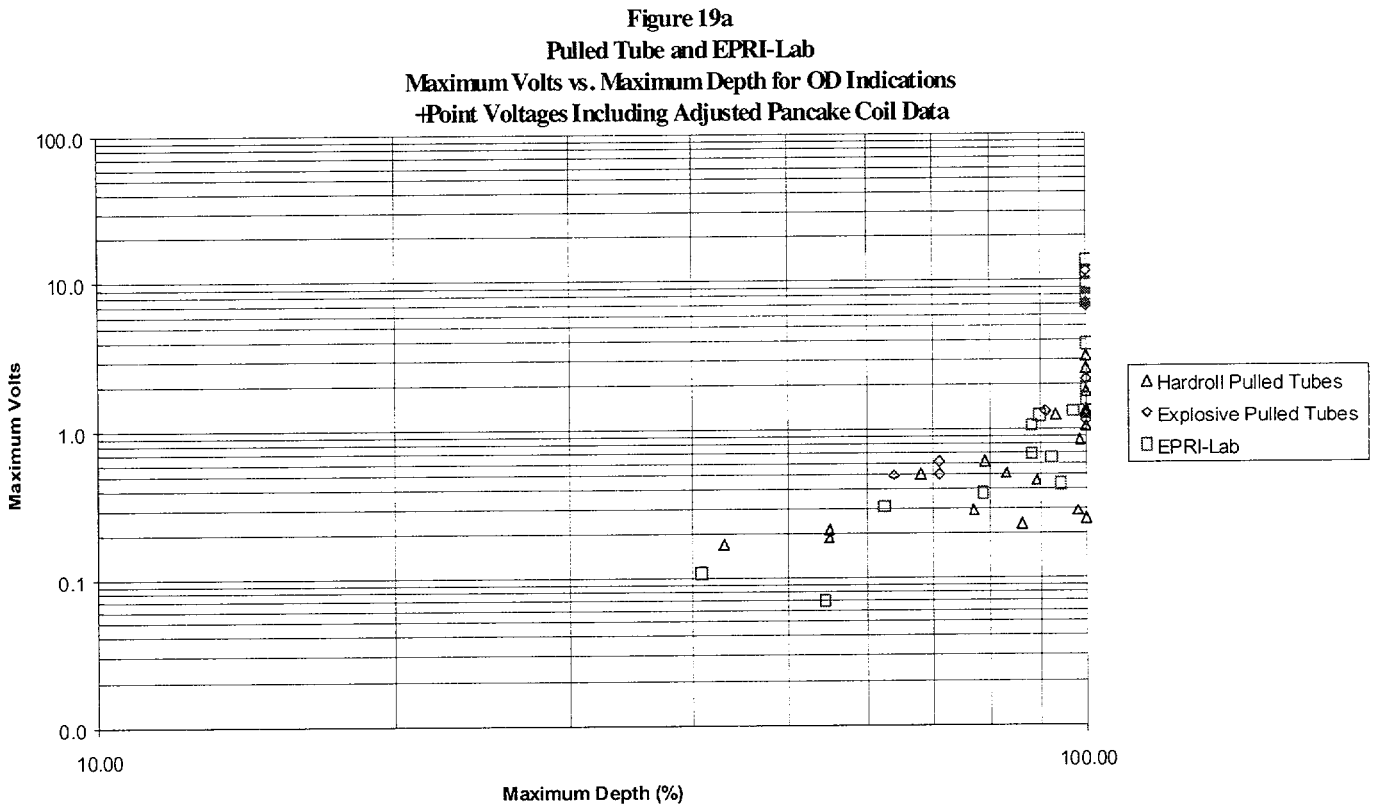

Reproduced from Figure G-15a contained in Appendix G of Electric Power Research Institute (EPRI) Report TR-107197-P2, "Depth Based Structural Analysis Methods for SG Circumferential Indications," dated December 1997, an EPRI licensed product.

Figure 19b

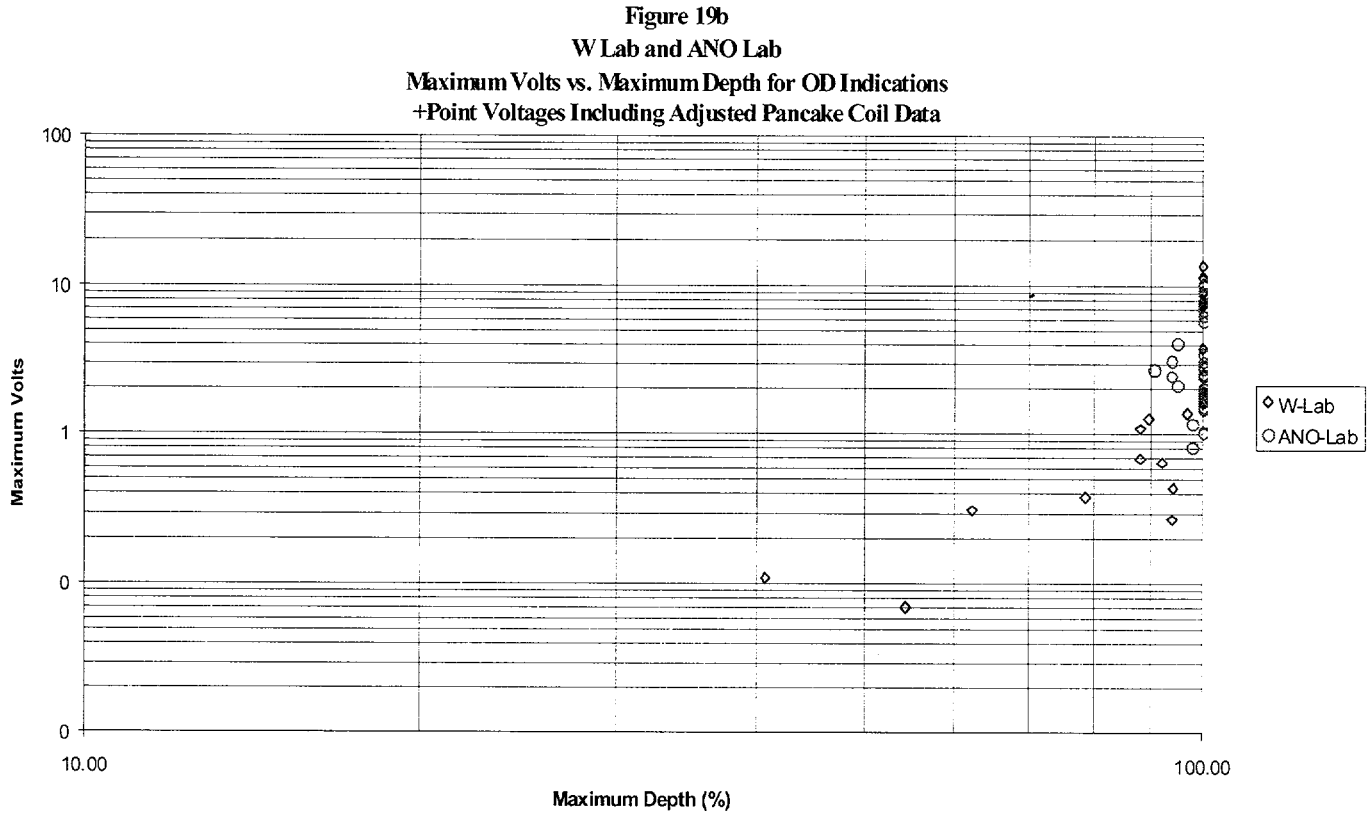

Reproduced from Figure G-15b contained in Appendix G of Electric Power Research Institute (EPRI) Report TR-107197-P2, "Depth Based Structural Analysis Methods for SG Circumferential Indications," dated December 1997, an EPRI licensed product.